Atypical connectome topography and signal flow in temporal lobe epilepsy

Ke Xie [a], Jessica Royer [a,b], Sara Larivière [a], Raul Rodriguez-Cruces [a], Stefan Frässle [c], Donna Gift Cabalo [a], Alexander Ngo [a], Jordan DeKraker [a], Hans Auer [a], Shahin Tavakol [a], Yifei Weng [d], Chifaou Abdallah [b], Thaera Arafat [a], Linda Horwood [a,b], Birgit Frauscher [b,e], Lorenzo Caciagli [f,g,h], Andrea Bernasconi [i], Neda Bernasconi [i], Zhiqiang Zhang [d], Luis Concha [j], Boris C. Bernhardt [a,*]

[a] Multimodal Imaging and Connectome Analysis Laboratory, McConnell Brain Imaging Centre, Montreal Neurological Institute and Hospital, McGill University, Montreal, QC H3A 2B4, Canada
[b] Analytical Neurophysiology Laboratory, Montreal Neurological Institute and Hospital, McGill University, Montreal, QC H3A 2B4, Canada
[c] Translational Neuromodeling Unit (TNU), Institute for Biomedical Engineering, University of Zurich and ETH Zurich, Zurich, Switzerland
[d] Department of Medical Imaging, Jinling Hospital, Nanjing University School of Medicine, Nanjing, China
[e] Department of Neurology, Duke University School of Medicine and Department of Biomedical Engineering, Duke University Pratt School of Engineering, Durham, NC 27705, USA
[f] Department of Bioengineering, University of Pennsylvania, Philadelphia, PA 19104, USA
[g] Department of Neurology, Inselspital, Sleep-Wake-Epilepsy-Center, Bern University Hospital, University of Bern, Bern, Switzerland
[h] Department of Clinical and Experimental Epilepsy, UCL Queen Square Institute of Neurology, London WC1N 3 BG, United Kingdom
[i] Neuroimaging of Epilepsy Laboratory, McConnell Brain Imaging Centre, Montreal Neurological Institute and Hospital, McGill University, Montreal, QC H3A 2B4, Canada
[j] Institute of Neurobiology, Universidad Nacional Autónoma de Mexico (UNAM), Queretaro, Mexico

ARTICLE INFO

ABSTRACT

Temporal lobe epilepsy (TLE) is the most common pharmaco-resistant epilepsy in adults. While primarily associated with mesiotemporal pathology, recent evidence suggests that brain alterations in TLE extend beyond the paralimbic epicenter and impact macroscale function and cognitive functions, particularly memory. Using connectome-wide manifold learning and generative models of effective connectivity, we examined functional topography and directional signal flow patterns between large-scale neural circuits in TLE at rest. Studying a multisite cohort of 95 patients with TLE and 95 healthy controls, we observed atypical functional topographies in the former group, characterized by reduced differentiation between sensory and transmodal association cortices, with most marked effects in bilateral temporo-limbic and ventromedial prefrontal cortices. These findings were consistent across all study sites, present in left and right lateralized patients, and validated in a subgroup of patients with histopathological validation of mesiotemporal sclerosis and post-surgical seizure freedom. Moreover, they were replicated in an independent cohort of 30 TLE patients and 40 healthy controls. Further analyses demonstrated that reduced differentiation related to decreased functional signal flow into and out of temporolimbic cortical systems and other brain networks. Parallel analyses of structural and diffusion-weighted MRI data revealed that topographic alterations were independent of TLE-related cortical thinning but partially mediated by white matter microstructural changes that radiated away from paralimbic circuits. Finally, we found a strong association between the degree of functional alterations and behavioral markers of memory dysfunction. Our work illustrates the complex landscape of macroscale functional imbalances in TLE, which can serve as intermediate markers bridging microstructural changes and cognitive impairment.

1. Introduction

Temporal lobe epilepsy (TLE) is the most prevalent pharmaco-resistant epilepsy in adults (Téllez-Zenteno and Hernández-Ronquillo, 2012). It is commonly considered a 'focal' syndrome with a mesio-temporal pathological core (Blümcke et al., 2013), but increasing

histopathological and neuroimaging evidence suggests the presence of widespread structural and functional alterations (Larivière et al., 2020a, 2022; Royer et al., 2022a; Stasenko et al., 2022; Whelan et al., 2018). These findings align with contemporary theories of brain pathology, indicating that disease-related anomalies are rarely confined to a single region, but often affect interconnected networks (Fornito et al., 2015). Therefore, a detailed understanding of brain network organization is crucial for capturing TLE-related pathophysiology at a system level. Previous studies, either carried out in single (Bernhardt et al., 2016, 2010, 2011; Yasuda et al., 2015) or multiple sites (Hatton et al., 2020; Larivière et al., 2022; Park et al., 2021b; Whelan et al., 2018), have established widespread structural network reorganization in TLE, involving both gray and white matter structural compromise. On the other hand, despite prior research demonstrating abnormal intrinsic functional connectivity in TLE at the level of single regions or networks using resting-state functional magnetic resonance imaging (rs-fMRI) (Bernhardt et al., 2016; Gonzalez et al., 2019; Maccotta et al., 2013; Sainburg et al., 2022), large-sale functional reorganization in this condition remains less well understood. Since macroscale imbalances compromise brain health, psychosocial function, and well-being (Hermann et al., 2021; Lin et al., 2012; Rodriguez-Cruces et al., 2022), there is a need to comprehensively assess functional connectome architecture in TLE.

Brain connectivity at the level of inter-regional edges between all regions is inherently high-dimensional, which challenges a synoptic visualization and synthesis of disease-related perturbations. This complexity also renders it difficult to contextualize findings in relation to established regional neuroimaging markers, including cortical morphology (Larivière et al., 2020a; Whelan et al., 2018) and superficial white matter microstructure (Anny et al., 2019; Hatton et al., 2020; Liu et al., 2016b). Recent conceptual and methodological advances have enabled the decomposition of whole-brain connectomes into a series of low-dimensional manifolds (*i.e.,* topological gradients) that capture the spatial trends of connectivity differentiation along the cortical mantle (Margulies et al., 2016). In contrast to graph theoretical approaches (Bassett and Sporns, 2017; Bassett et al., 2018; Bernhardt et al., 2015; Bullmore and Sporns, 2009) or clustering-based decompositions of the brain into discrete communities (Yeo et al., 2011), gradient mapping techniques describe a continuous representation of brain organization, allowing for the identification of fine-grained changes in specific brain regions. Prior investigations have established that connectome gradients derived from resting-state functional, diffusion-weighted, and microstructural MRI spatially co-localized with the principal axes of laminar differentiation and gene expression (Burt et al., 2018; Goulas et al., 2021; Margulies et al., 2016; Paquola and Hong, 2022), linking brain macroscale organization to molecular signatures. Gradient mapping techniques, thus, provide a biologically plausible perspective on large-scale connectome configurations in a data-driven and spatially unconstrained manner. This framework has been recently applied in the study of neuro-development (Dong et al., 2021; Park et al., 2022; Sydnor et al., 2023), structure-function coupling (Paquola et al., 2019; Valk et al., 2022), as well as the assessment of conditions involving atypical brain function, including autism (Hong et al., 2019b; Park et al., 2021a), major depressive disorder (Xia et al., 2022), and generalized epilepsy (Meng et al., 2021). In the case of TLE, connectome gradient analyses have been applied to high-resolution quantitative T1 relaxometry and task-based functional MRI during memory paradigms, revealing microstructural miswiring and state-specific functional reorganization (Caciagli et al., 2022; Li et al., 2021; Royer et al., 2023). There has also been a recent characterization of subcortical functional gradients in TLE, showing alterations in functional organization that varied as a function of seizure focus laterality (Lucas et al., 2023b). In this study, we expanded upon these findings by examining the reorganization of intrinsic functional topographies of the cerebral cortex in TLE. The low-dimensional insights offered by spatial gradients also allowed for the integration of connectome-level findings with changes in regional

morphology and microstructure estimated from structural and diffusion MRI measures (Bernhardt et al., 2009; Hatton et al., 2020; Larivière et al., 2020a; Liu et al., 2016b; Whelan et al., 2018), thus allowing for the assessment of structure-function coupling alterations.

While the analysis of connectome gradients provides a concise mapping of functional topographies, it does not *per se* tap into directional signal flow that is key to cortical hierarchical organization (Gu et al., 2021; Raut et al., 2021; Yousefi and Keilholz, 2021). Cortical hierarchy is thought to constrain bottom-up information flow from sensory systems to transmodal systems, as well as top-down modulation in the opposite direction (Markov et al., 2013, 2014; Markov and Kennedy, 2013; Vezoli et al., 2021). Consequently, changes in connectivity that result in hierarchical imbalances will affect information flow (Hong et al., 2019b), as hypothesized in TLE (Girardi-Schappo et al., 2021). To complement gradient-informed findings, we employed regression dynamic causal modeling (rDCM) (Frässle et al., 2018, 2017; Frassle et al., 2021b), a recently developed generative model of effective connectivity. Expanding upon the classical dynamic causal modeling framework, rDCM is computationally efficient when dealing with large networks comprising hundreds of nodes (Friston et al., 2014). Moreover, when applied to rs-fMRI data, rDCM exhibits high construct validity and test-retest reliability (Frassle et al., 2021a; Frassle and Stephan, 2022), making it a potentially valuable tool for mapping atypical signal flow in disease.

Our goal was to uncover perturbations in macroscale cortical hierarchy in individuals with TLE and explore their associations with structural compromise and cognitive deficits. Leveraging a large, multi-site cohort of TLE patients and controls, we characterized intrinsic functional topography using non-linear connectome compression techniques and identified patterns of signal flow using rDCM. Furthermore, we explored associations with TLE-related alterations in gray matter morphology and white matter microstructure. Finally, we evaluated whether these functional changes were related to impairments across various cognitive domains, as assessed by behavioral batteries. Although our study was data-driven and regionally unconstrained, TLE patients were expected to exhibit atypical functional organization at a system level. In particular, mirroring effects in other neurodevelopmental conditions (Hong et al., 2019b; Xia et al., 2022), TLE was likely associated with an atypical functional differentiation between transmodal and unimodal regions, which would manifest in altered functional topographic gradient organization as well as aberrant signal flow. Given prior work showing that large-scale effects in TLE often aggregate within temporo-limbic epicenters, we equally expected to identify atypical functional organization in these regions. Our primary analysis was conducted in a discovery cohort of 190 individuals (95 TLE patients and 95 age- and sex-matched healthy controls) aggregated from three independent sites. The generalizability of our findings was then assessed in a replication cohort of 70 individuals (30 TLE patients and 40 healthy controls).

2. Materials and Methods

2.1. Participants

Our discovery dataset contained a total of 190 individuals, including 95 patients with pharmaco-resistant unilateral TLE (43 males; mean age $\pm$ SD = 31.19 $\pm$ 10.57 years) and 95 age- and sex-matched healthy controls (45 males; 31.53 $\pm$ 8.37 years). All participants were aged between 18–58 years. There were no significant differences in age ($t =$ 0.24, $P = 0.808$) and sex ($\chi^2 = 0.08$, $P = 0.771$) between two groups. Average age at seizure onset was 16.68 $\pm$ 9.74 years, and average duration of illness was 14.25 $\pm$ 11.42 years. Participants were selected from three independent sites: (i) Montreal Neurological Institute and Hospital (*MICA-MICs*; $n = 75$) (Royer et al., 2022b), (ii) Universidad Nacional Autonoma de Mexico (*EpiC*; $n = 50$) (Rodriguez-Cruces et al., 2020), and (iii) Jinling Hospital, China (*NKG*; $n = 65$) (Weng et al.,

2020). Patients were diagnosed according to the ILAE classification based on a comprehensive evaluation includes clinical history, seizure semiology, video-EEG recordings, neuropsychological assessment, and clinical MRI. The study was approved by local ethics committees, and all participants provided written informed consent in accordance with the Declarations of Helsinki. Site-specific demographic and clinical information can be found in Table 1.

We further evaluated an independent replication dataset of 30 pharmaco-resistant TLE patients (18 males; 30.83 ± 9.35 years), and 40 age- and sex-matched healthy controls (20 males; 26.68 ± 5.68 years) recruited at the *NKG* site. All participants were aged between 18–48 years. A similar evaluation classified them as unilateral left ($n = 11$) or right TLE ($n = 19$). Detailed demographic and clinical information can be found in Table S1.

2.2. MRI Acquisition

All participants underwent multimodal MRI data acquisitions, including T1-weighted MRI, rs-fMRI, and diffusion-weighted imaging (DWI). In *EpiC*, data were acquired on a 3 T Philips Achieva scanner, and included (i) a T1-weighted scan (3D spoiled gradient-echo, voxel size = $1 \times 1 \times 1$ mm^3, TR = 8.1 ms, TE = 3.7 ms, FA = 8°, FOV = 256×256 mm^2), (ii) a rs-fMRI scan (gradient-echo EPI, voxel size = $2 \times 2 \times 3$ mm^3, TR = 2000 ms, TE = 30 ms, FA = 90°, 34 slices, 200 volumes), and (iii) a DWI scan (2D EPI, voxel size = $2 \times 2 \times 2$ mm^3, TR = 11.86 s, TE = 64.3 ms, FOV = 256×256 mm^2, 2 b0 images, b-value = 2000 s/mm^2, 60 diffusion directions). In *MICA-MICs*, data were acquired on a 3 T Siemens Magnetom Prisma-Fit scanner, and included: (i) two T1-weighted scans (3D-MPRAGE, voxel size = $0.8 \times 0.8 \times 0.8$ mm^3, matrix size = 320×320, TR = 2300 ms, TE = 3.14 ms, FA = 9°, TI = 900 ms, FOV = 256×256 mm^2), (ii) a rs-fMRI scan (multiband accelerated 2D-BOLD EPI, voxel size = $3 \times 3 \times 3$ mm^3, TR = 600 ms, TE = 30 ms, FA = 52°, FOV = 240×240 mm^2, multi-band factor = 6, 48 slices, 700 volumes), and (iii) a multi-shell DWI scan (2D EPI, voxel size = $1.6 \times 1.6 \times 1.6$ mm^3, TR = 3500 ms, TE = 64.4 ms, FA = 90°, FOV = 224×224 mm^2, 3 b0 images, b-values = 300/700/2000 s/mm^2, 10/40/90 diffusion directions). In *NKG*, data were acquired on a 3 T Siemens Trio scanner, and included (i) a T1-weighted scan (3D-MPRAGE, voxel size = $0.5 \times 0.5 \times 1$ mm^3, TR = 2300 ms, TE = 2.98 ms, FOV = 256×256 mm^2, FA = 9°), (ii) a rs-fMRI scan (2D echo-planar BOLD, voxel size = $3.75 \times 3.75 \times 4$ mm^3, TR = 2000 ms, TE = 30 ms, FA = 90°, FOV = 240×240 mm^2, 30 slices, 255 volumes), and (iii) a DWI scan (2D EPI, voxel size = $0.94 \times 0.94 \times 3$ mm^3, TR = 6100 ms, TE = 93 ms, FA = 90°, FOV = 240×240 mm^2, 4 b0 images, b-value = 1000 s/mm^2, 120 diffusion directions).

2.3. MRI Processing

Multimodal processing utilized *micapipe* (version 0.1.4; http://micapipe.readthedocs.io) (Cruces et al., 2022), an open-access pipeline that integrates AFNI, FSL, FreeSurfer, ANTs, and Workbench (Avants et al., 2011; Cox, 1996; Fischl, 2012; Glasser et al., 2013; Jenkinson et al., 2012). T1-weighted data were de-obliqued, reoriented, linearly co-registered, intensity non-uniformity corrected, and skull stripped. FreeSurfer 6.0 was used to generate models of the inner and outer cortical interfaces, with manual correction of segmentation errors. Native cortical features were registered to the Conte69 template surface (~32k vertices/hemisphere). Cortical thickness, measured as the Euclidean distance between corresponding pial and white matter vertices, was computed for each participant, and then registered to Conte69 (Van Essen et al., 2012). DWI data were denoised, corrected for susceptibility distortions, head motion, and eddy currents. A Laplacian potential field was used to guide the placement of a superior white matter (SWM) surface, targeting a depth of ~2 mm beneath the gray-white matter boundary to capture the U-fibre system and the terminations of long-range bundles located between 1.5 and 2.5 mm beneath the cortical interface, following the approach used in previous studies (Hong et al., 2019a; Larivière et al., 2020b; Liu et al., 2016b). Diffusion features, fractional anisotropy (FA) and mean diffusivity (MD), which served as surrogates of fibre architecture and tissue microstructure, were linearly interpolated along the SWM surface and registered to Conte69. rs-fMRI processing included discarding the first five volumes, reorientation, slice-timing correction (*EpiC* and *NKG*), and head motion correction. Nuisance signals were removed using an in-house trained ICA-FIX classifier (Salimi-Khorshidi et al., 2014). Preprocessed time series were non-linearly registered to native FreeSurfer space using boundary-based registration and resampled to Conte69 (Greve and Fischl, 2009). Surface-based maps, including cortical thickness, FA, MD, and rs-fMRI time series, underwent spatial smoothing (full-width-at-half-maximum = 10 mm). Lastly, vertex-wise maps were downsampled using the Glasser atlas (Glasser et al., 2016), a multimodal parcellation comprising 180 homologous parcels per hemisphere.

2.4. Connectome Gradient Analysis

Cortex-wide functional connectome gradients were generated using BrainSpace (version 0.1.10; https://github.com/MICA-MNI/BrainSpace) (Vos de Wael et al., 2020). Pearson's correlations of time series between each pair of regions were calculated, resulting a 360×360 functional connectome matrix per participant. Similar to previous studies (Margulies et al., 2016), we retained the top 10% weighted connections per region after z-transforming the data. An

Table 1
Demographic and clinical information of the discovery dataset.

	EpiC Site			*MICA-MICs* Site			*NKG* Site		
	HC	TLE	*P*	HC	TLE	*P*	HC	TLE	*P*
Number	25	25	-	40	35	-	30	35	-
Age	31.8±12.2 (18–57)	30.8±11.7 (18–58)	0.75[a]	34.4±3.9 (29–44)	35.7±10.7 (18–57)	0.48[a]	27.5±7.4 (19–40)	27.0±7.8 (18–43)	0.82[a]
Sex (M/F)	14/11	10/15	0.78[b]	20/20	16/19	0.71[b]	14/16	17/18	0.88[b]
Side of focus (L/R)	-	15/10	-	-	25/10	-	-	15/20	-
Age at onset	-	13.5±10.0 (0.7–40)	-	-	20.4±10.2 (0.5–49)	-	-	15.2±8.0 (1–28)	-
Duration of illness	-	17.3±13.8 (1–49)	-	-	15.2±12.3 (1–45)	-	-	11.1±7.6 (0.2–29.7)	-
HA, n (%)	-	15 (60)	-	-	19 (54)	-	-	32 (91)	-
Surgery (Engel I)	-	-	-	11 (8)[c]	-	-	35 (24)[c]	-	-

Abbreviations: HC, healthy control; TLE, temporal lobe epilepsy; M, male; F, female; L, left; R, right; HA, hippocampal atrophy (percentage of patients in the group), determined as the absolute hippocampal volumes or inter-hemispheric asymmetry (ipsilateral - contralateral) beyond 2 SDs of the corresponding mean of healthy controls (Bernasconi et al., 2003). Age, age at seizure onset, and duration of illness are presented as mean ± SD years. [a] Two-sample t-test. [b] Chi-square test. [c] Engel I: seizure-free, *i.e.,* Class I postsurgical outcome in Engel's classification.

affinity matrix was constructed using a normalized angle kernel to capture the similarity in connectivity profiles between regions (Park et al., 2021c). To identify gradient components that explained the variance in the connectivity profiles of the functional connectome, we employed diffusion map embedding, a robust and computationally efficient non-linear manifold learning technique (Coifman et al., 2005; Margulies et al., 2016). We set the values of α and t to 0.5 and 0, respectively, to retain global relations between data points in the embedded space, as done in previous studies (Hong et al., 2019b; Margulies et al., 2016; Vos de Wael et al., 2020). Individual-level gradient maps were aligned to template gradients generated from 100 unrelated healthy adults from the Human Connectome Project (HCP) database using Procrustes rotation, following prior work (Li et al., 2021; Park et al., 2021b; Wang et al., 2022). The MRI parameters and processing details of the HCP dataset can be found in refs (Glasser et al., 2013; Van Essen et al., 2013). The HCP dataset was chosen due to its high-quality imaging data and its common use for constructing brain atlases (Glasser et al., 2016), as well as for building reference templates for gradient alignment and contextualization (Paquola et al., 2019; Park et al., 2021b; Vos de Wael et al., 2020; Wang et al., 2022).

To quantify between-group differences in functional gradient values between TLE patients and controls, we z-scored the principal functional gradient maps in patients with respect to site-matched controls and sorted them into ipsilateral/contralateral to the focus (Liu et al., 2016a). Surface-based linear models, implemented in BrainStat (version 0.4.2; https://brainstat.readthedocs.io) (Larivière et al., 2023), were used to compare the groups, with age, sex, and site included as covariates. Cohen's d effect sizes were calculated to determine the magnitude of between-group differences. To account for multiple comparisons, a false discovery rate (FDR) procedure was applied (Benjamini and Hochberg, 1995). Additionally, we stratified the functional gradient findings with respective to twelve macroscale functional networks defined on the Glasser atlas, using the Cole-Anticevic Brain-Wide Network Partition (Ji et al., 2019).

Post-hoc analyses were carried out to evaluate the consistency of TLE-related gradient changes across the three sites in the discovery dataset. Firstly, as in previous MRI analyses (Valk et al., 2015), we calculated the average gradient values within the clusters showing significant gradient changes in the main multisite analysis and compared them between healthy control and TLE groups within each of the three sites separately. This allowed us to evaluate the effect sizes of functional gradient changes at each site at a cluster-specific level. Secondly, we repeated the cortex-wide gradient comparison between groups at each site, while controlling for age and sex. This analysis aimed to assess the effect sizes of between-group differences in the principal functional gradient values at each brain area and each site independently. Cortex-wide consistency between sites was defined as the spatial correlations of site-specific TLE-control effect size maps (*i.e.*, Cohen's d maps) (Anderson et al., 2020; Ji et al., 2022; Xie et al., 2023). The significance of these correlations was determined using spin permutation tests with 5000 iterations, which preserved the spatial autocorrelation of the original data (here P values were denoted as P_{spin}) (Alexander-Bloch et al., 2018; Lariviere et al., 2021; Váša and Mišić, 2022).

2.5. Effective Connectivity Analysis

To examine the directed functional flow to and from regions showing significant gradient alterations, we employed rDCM, a scalable and computationally efficient generative model of whole-brain effective connectivity from rs-fMRI (Frässle et al., 2021, 2017; Frassle et al., 2021a). Compared to the conventional dynamic causal modelling framework (Friston et al., 2014), rDCM (i) translates state and observation equations of a linear dynamic causal model from the time to the frequency domain, (ii) substitutes the non-linear hemodynamic model with a linear hemodynamic response function, (iii) implements a mean-field approximation across regions (*i.e.,* parameters targeting

different regions are assumed to be independent), and (iv) specifies conjugate priors on the noise precision, connectivity, and driving input parameters (Frassle et al., 2021a; Frassle and Stephan, 2022). These modifications essentially reframe a linear DCM in the time domain as a Bayesian linear regression in the frequency domain. As a result, rDCM can be scaled to large networks comprising hundreds of nodes, allowing for the estimation of effective connectivity from rs-fMRI at the whole-brain level. A more detailed description of rDCM, including the mathematical details of the neuronal state equations, can be found elsewhere (Frässle et al., 2018, 2017). These modifications essentially reframe a linear DCM in the time domain as a Bayesian linear regression in the frequency domain. As a result, rDCM can be scaled to large networks comprising hundreds of nodes, allowing for the estimation of effective connectivity at the whole-brain level. A comprehensive description of rDCM, including the mathematical details of the neuronal state equations, can be found elsewhere in refs (Frässle et al., 2018, 2017; Frassle et al., 2021b; Frassle and Stephan, 2022).

Time series derived from preprocessed rs-fMRI data were utilized for the whole-brain effective connectivity estimation for each individual, through a fully connected network architecture of rDCM (Fig. 2a), implemented in TAPAS (version 6.0.1; https://www.tnu.ethz.ch/de/software/tapas) (Frässle et al., 2021). The resulting subject-specific effective connectivity matrix (360×360, including 129, 240 connectivity parameters and 360 inhibitory self-connections) was divided into an efferent component (*i.e.,* columns in Fig. 2b), reflecting outward signal flow, and an afferent component (*i.e.,* rows in Fig. 2b), reflecting inward flow. Weighted outward and inward degree measures were computed for each node, representing the sum of the unsigned efferent and afferent connectivity weights, respectively (Zuo et al., 2012). To capture overall alterations in signal flows, we compared the aggregate of outward-degree and inward-degree values between TLE patients and healthy controls using multivariate surface-based linear models. *Post-hoc* univariate models were employed to identify specific patterns of outward-degree or inward-degree differences between both groups.

To interrogate whether signal flow perturbations can account for gradient alterations, we repeated the surface-wide between-group comparisons of the principal functional gradient while additionally controlling for the node-wise outward- and inward-degree measures. Furthermore, we calculated the average outward- and inward-degree values within brain regions with significant gradient changes, and correlated them with subject-specific average functional gradient values in the same regions in healthy control and TLE groups separately. This analysis aimed to explore the association between functional gradient alterations and signal flow changes within specific brain regions.

2.6. Assessment of Morphological and Microstructural Substrates

We carried out several analyses to explore the associations of functional gradient changes, cortical morphology, and SWM microstructure. Firstly, we performed surface-based linear models to assess morphological and microstructural indices between TLE patients to controls, while controlling for effects of age, sex, and site as covariates. Secondly, we examined TLE-related gradient changes above and beyond structural changes by comparing the principal functional gradient values between groups while also controlling for cortical thickness or diffusion parameters at each region. Furthermore, we conducted statistical mediation analyses to quantify the extent to which cortical morphological and SWM microstructural changes contributed to functional gradient changes. The mediation models included the principal functional gradient values (*gradient*) as the dependent variable, *group* (*i.e.,* TLE vs. controls) as the predictor, and cortical structure (*structure*), including cortical thickness, or fractional anisotropy (FA), or mean diffusivity (MD), as the mediator. For each participant, we calculated the average cortical thickness, FA, MD, and functional gradient values within clusters showing significant gradient reductions (refer to Fig. 1d). The
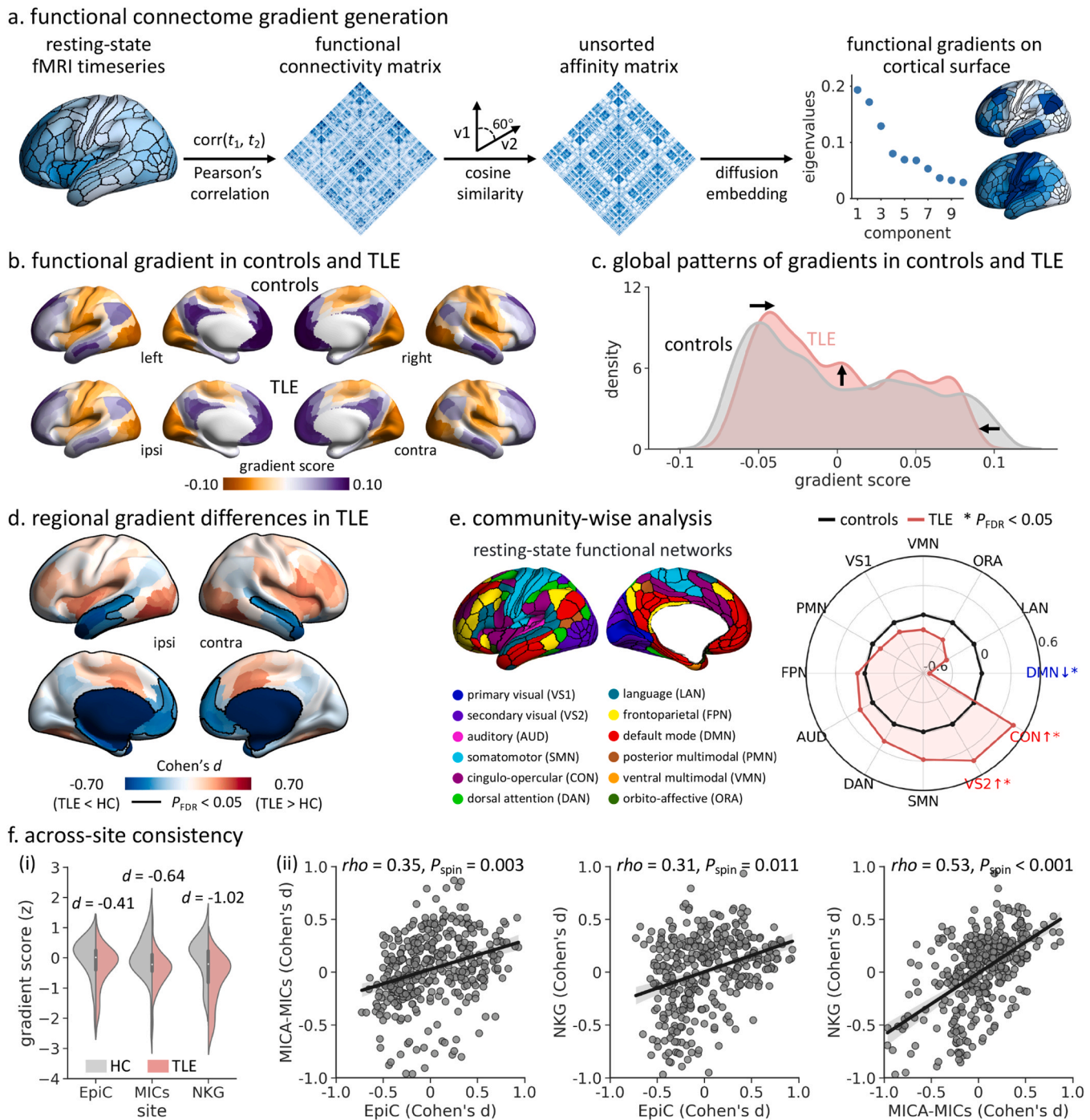
Fig. 1. Between-group differences in the principal functional gradient. **(a)** A schematic of functional connectivity gradient mapping. **(b)** The principal gradient in healthy controls ($n = 95$) and patients with TLE ($n = 95$). **(c)** Global histograms indicated that the two anchors of the gradient were contracted in TLE compared to healthy controls. **(d)** Surface-based linear models, controlling for age, sex, and site, showed regional differences in the principal gradient between groups. Significant clusters, corrected for multiple comparisons using the false discovery rate procedure, are outlined in black ($P_{FDR} < 0.05$). **(e)** Community-wise analysis revealed reduced gradient values predominantly in the default-mode network (DMN) and increases in the secondary visual network (VS2) and cingulo-opercular network (CON) in TLE ($P_{FDR} < 0.05$). **(f)** Across-site consistency. **(i)** Site-specific between-group differences in the mean gradient values within regions showing significant gradient changes. **(ii)** Across-site spatial correlations of between-group effect size maps (*i.e.,* unthresholded Cohen's d maps), with each dot representing the Cohen's d effect size from one region. Statistical significance of spatial correlations (*i.e.,* P_{spin}) was evaluated using 5000 spin permutation tests to account for the spatial autocorrelation (Alexander-Bloch et al., 2018; Lariviere et al., 2021; Váša and Mišić, 2022). Abbreviations: *HC*, healthy controls; *TLE*, temporal lobe epilepsy; *ipsi*, ipsilateral; *contra*, contralateral.

mediation models involved four paths: (i) path *a*, representing the relationship between *group* and *structure*; (ii) path *b*, representing the relationship between *structure* and *gradient*; (iii) path *c'*, representing the direct effect of *group* on *gradient* while controlling for the mediator

structure; and (iv) the mediation/indirect effect ($a \times b$), representing the effect of the relationship between *group* and *gradient* that was reduced after accounting for *structure*. Significance of paths was determined using bootstrapped confidence intervals (10,000 times), implemented in

the MediationToolbox (version 1.0.0; https://github.com/canlab/MediationToolbox).

2.7. Associations with Cognitive Variables

At the *MICA-MICs* site, participants engaged in three memory tasks (semantic, episodic, and spatial) while inside the scanner (Shahin et al., 2022; Tavakol et al., 2021), as well as the EpiTrack test outside the scanner (Lutz and Helmstaedter, 2005). The semantic task required participants to identify the item that was conceptually most similar to the target in a 3-alternative forced-choice design. A total of 56 pseudo-randomized trials were administered, consisting of 28 easy trials (Sem-E) and 28 difficult trials (Sem-D). The UMBC index (range: 0–1), measuring the semantic relatedness of items (Han et al., 2013), was 0–0.3 between the foils and target in Sem-E trials, and 0.3–0.7 in Sem-D trials (Tavakol et al., 2021). The episodic task consisted of two phases. Participants were presented with pairs of images simultaneously and then, following a 10-minute delay, had to identify the original object item that was paired with the target from the encoding phase in a 3-alternative forced-choice design (Tavakol et al., 2021). A total of 56 pseudo-randomized trials were administered, with 28 trials corresponding to pairs of images encoded only once (Epi-D) and 28 trials corresponding to pairs of images encoded twice (Epi-E). The UMBC index for each pair was smaller than 0.3. In the spatial task, also comprising two phases, participants were required to memorize the spatial arrangement of 3 semantically unrelated items (UMBC index < 0.3) and discriminate the original layout from two additional foil layouts of the same items, with a jittered interval of 0.5–1.5 seconds (Tavakol et al., 2021). The task included 56 pseudo-randomized trials, with 28 trials categorized as easy (Spa-E) and 28 trials categorized as difficult (Spa-D). In Spa-D trials, the foil layouts differed from the original one by 2 degrees of separation (*e.g.*, rotation about the center of mass and spacing alteration), while in Spa-E trials, the foil layouts involved 3 degrees of separation (*e.g.*, rotation about the center of mass, spacing alteration, and item positional swap). After excluding participants with incomplete data ($n = 12$), a total of 63 participants were included in the analysis (38 controls and 25 patients). Experiment scripts and stimuli are available at http://github.com/MICA-MNI/micaopen/.

At the *EpiC* site, participants underwent the Wechsler Memory Scale (WMS-IV) test, which consisted of 7 subtests designed to assess memory performance (Rodriguez-Cruces et al., 2018). The WMS-IV derived 5 indices: auditory memory (AMI), visual memory (VMI), visual working memory (VWMI), immediate memory (IMI), and delayed memory (DMI). These indices were normalized based on a Mexican population, and adjusted for age and education level. After excluding participants with incomplete data ($n = 5$), a total of 45 participants were included in the analysis (20 controls and 25 patients). No cognitive data were available for the *NKG* site.

We investigated the relationship between participants' cognitive performance and functional network metrics. For each participant, we calculated the mean functional gradient, outward-degree, and inward-degree values within regions with significant gradient changes. Cognitive performance indices were z-scored and fed to a principal component analysis (PCA) to reduce dimensionality. We then correlated the principal component score (PC1) which represented overall memory performance, with each of the three imaging measures while controlling for age and sex. Additionally, we constructed a multiple linear regression model to examine the combined effects of all three imaging measures (*i.e.*, PC1 ~ gradient + outward-degree + inward-degree). These analyses were conducted separately at *MICA-MICs* and *EpiC* sites. To assess the specificity of brain-memory associations, we further examined correlations between individual EpiTrack score which reflected attention and executive functions (available only at the *MICA-MICs* site), and the imaging measures.

2.8. Cognitive Decoding based on Neurosynth

To explore the cognitive associations of brain regions showing TLE-related gradient changes, we conducted a functional decoding analysis using Neurosynth (https://neurosynth.org/, December 2020 release), a platform for *ad hoc* meta-analysis of task-based functional MRI data (Yarkoni et al., 2011). In briefly, the FDR-corrected brain regions derived from between-group comparisons of the principal functional gradient (Fig. 1d) were used as input for a "decoder" wrapper implemented in BrainStat (Larivière et al., 2023). We specifically focused on cognitive and disorder-related terms and excluded anatomical and demographic terms in our analysis.

2.9. Sensitivity, Robustness, and Replication Analyses

2.9.1. Left and Right TLE
To account for the potential effect of focus lateralization on the topological organization of functional networks, we separately conducted surface-wide between-group comparison of the principal functional gradient for left ($n_{\text{LTLE}} = 55$) and right TLE patients ($n_{\text{RTLE}} = 40$). We then computed spatial correlations of effect sizes (*i.e.*, Cohen's d) between these two subgroups. Additionally, we performed two-sample t-tests to compare directly the mean functional gradient values within significant regions identified in the multisite aggregation analyses (Fig. 1d) between the left/right TLE group and the healthy control group.

2.9.2. Seizure-Free TLE
To ensure the validity of our findings, we selected those patients who had undergone surgery after our initial investigation, had histologically confirmed mesiotemporal pathology, and were seizure-free at follow-up (*i.e.*, Engel I: *MICA-MICs* site, $n = 8$; *NKG* site, $n = 24$). We reanalysed functional connectome gradients using the same methodology as before, comparing this specific subgroup of patients to controls.

2.9.3. Head Motion and tSNR Effects
To confirm that the main gradient findings were not related to fMRI-related related artifacts, we calculated the degree of head motion (framewise displacement, FD) during rs-fMRI scans and cortex-wide temporal signal-to-noise ratio (Murphy et al., 2013; Power et al., 2014). We repeated surface-wide between-group comparisons of the functional gradients while including subject-specific mean FD or regional signal-to-noise ratio estimates as covariates to account for their potential effects.

2.9.4. Connectivity Matrix Thresholding
To evaluate the effects of connectivity matrix thresholding on our findings, we generated connectome gradients using matrices thresholded at various levels, specifically at 50%, 60%, 70%, and 80%. We repeated the surface-wide comparisons of newly defined functional gradients between TLE patients and controls and determined their consistency with the Cohen's d map from the default setting at 90%.

2.9.5. Age at Seizure Onset Effects
To mitigate the potential impact of variations in the age at seizure onset between the *MICA-MICs* site and the other sites, we performed surface-wide functional gradient comparisons between groups after excluding five TLE patients with a late age at seizure onset from this site (average age at seizure onset $= 17.45 \pm 6.82$ years, range $= 0.5$–27 years), thereby reducing the differences in age at seizure onset between the three sites we studied ($F_{(2,87)} = 1.61$, $P = 0.207$).

2.9.6. Interictal Epileptiform Discharges Effects
We furthermore explored associations between functional measures and the prevalence of inter-ictal epileptiform discharges (IEDs) in the temporal lobe in TLE patients at the *MICA-MICs* site who underwent

extended video-EEG telemetry as part of the in-patient investigations at our hospital (mean $\pm$ SD = 8.76 $\pm$ 2.70 days, range = 2–15 days). For each patient, we extracted the IEDs severity based on the classification obtained from the clinical EEG reports during hospitalization. Following the ACNS Critical Care EEG Terminology 2021 (Hirsch et al., 2021), TLE patients were subdivided into three groups: rare IEDs (<1/hour; n = 11), occasional IEDs ($\geq$1/hour but less than 1/minute; n = 10), and frequent/abundant IEDs ($\geq$1/minute; n = 12) (see IEDs localization in Table S2). The features of resting-state brain function described above were compared among these three subgroups using an analysis of variance (ANOVA).

2.9.7. Replication Analysis

We examined the reproducibility of our main findings using an independent dataset consisting of 30 individuals with pharmaco-resistant TLE and 40 age- and sex-matched healthy adults (see Table S1). We compared the principal functional gradient values between TLE and control groups following the procedure outlined above.

3. Results

3.1. Altered Topographic Gradients in TLE

We studied a multisite discovery dataset of patients with TLE and healthy controls, and applied non-linear dimensionality reduction techniques to cortex-wide functional connectomes derived from rs-fMRI data to estimate topographic gradients (Fig. 1a). The principal functional gradient, which accounted for 16.5 $\pm$ 1.3% of the total variance (TLE: 16.4 $\pm$ 1.3%; healthy controls, 16.5 $\pm$ 1.3%), demonstrated a gradual transition from unimodal sensory/motor to transmodal association systems in both groups (spatial map similarity: rho = 0.98, P_{spin} < 0.001; Fig. 1b), in line with earlier findings in healthy adults (Margulies et al., 2016).

Notably, the extremes of the gradient histogram were contracted in TLE patients compared to healthy controls (Fig. 1c), a finding further supported by surface-based comparisons. Specifically, TLE patients exhibited markedly lower functional gradient values in bilateral temporal and ventromedial prefrontal cortices relative to healthy controls (P_{FDR} < 0.05; mean $\pm$ SD Cohen's d in significant clusters: −0.46 $\pm$ 0.14; Fig. 1d). Stratifying the topography using a well-established functional atlas showed that TLE patients had lower functional gradient values in the default-mode network, and higher values in the secondary visual and cingulo-opercular networks (P_{FDR} < 0.05, Fig. 1e) (Ji et al., 2019). The consistency of these findings was demonstrated across the three sites included in our study. Gradient reductions in bilateral temporal and medial prefrontal cortices were consistent across the 3 sites, albeit with variable effect sizes (EpiC/MICA-MICs/NKG Cohen's d = −0.41/−0.64/−1.02). The spatial patterns of TLE-related gradient alterations were similar across sites (EpiC vs. MICA-MICs: rho = 0.35, P_{spin} = 0.003; EpiC vs. NKG: rho = 0.31, P_{spin} = 0.011; MICA-MICs vs. NKG: rho = 0.53, P_{spin} < 0.001; Fig. 1f and Figure S1).

3.2. Relation to Effective Connectivity Alterations

After characterizing topographic changes in TLE, we examined association between these findings and atypical functional signal flow. We utilized rDCM (Frassle et al., 2021a), a method that allowed us to estimate the cortex-wide effective connectivity from rs-fMRI data for each participant (Fig. 2a). We calculated the outward and inward degree centrality at a nodal level to quantify the flow of functional signals (see **2.5 Effective Connectivity Analysis**). The spatial distributions of outward- and inward-degree values across the entire neocortex were generally similar (rho = 0.54, P_{spin} < 0.001). Specifically, the lateral frontoparietal and medial occipital cortices showed relatively higher outward-degree values, indicating relatively stronger outflux signal flow; the temporolimbic cortex exhibited lower outward-degree values,

corresponding to weaker outflux flow. Inward-degree values, on the other hand, predominantly varied along the anterior-posterior axis of the neocortex, with occipito-parietal cortices exhibiting highest influx flow, while mesiotemporal and paralimbic cortices such as the orbito-frontal and anterior insula showed much lower flow (Fig. 2b).

Cortex-wide multivariate between-group comparisons, which aggregated outward- and inward-degree values, found significant alterations in TLE patients relative to healthy controls, primarily in a bilateral network encompassing the middle temporal gyri, insula, ventromedial and dorsolateral prefrontal cortices, as well as the contralateral central regions (P_{FDR} < 0.05; Fig. 2c). Univariate analyses indicated reduced outward-degree and inward-degree values in these regions in TLE patients (P_{FDR} < 0.05; Fig. 2c). To evaluate the shared effects of gradient and directed connectivity changes, we compared the principal functional gradient between groups using statistical models that also controlled for outward-degree and inward-degree values in each node. This analysis revealed reduced effect sizes of functional gradient reductions and less extended gradient changes in TLE, with only the bilateral temporal poles showing significant gradient changes following FDR-correction (P_{FDR} < 0.05; Figure S2). In a *post hoc* analysis focusing on regions showing significant gradient changes in TLE (Fig. 1d), we quantified the correlation between the principal functional gradient and directed connectivity changes. We calculated the average outward- and inward-degree values within these regions for each participant and correlated them with subject-specific mean functional gradient values in the same regions. Compared to healthy controls, TLE patients showed significant reductions in both outward- (Cohen's d = −0.27, P = 0.030) and inward-degree values (Cohen's d = −0.36, P = 0.005) (Fig. 2d). Furthermore, there was a positive correlation between functional gradient values and corresponding outward-degree (r = 0.24, P = 0.010) and inward-degree values (r = 0.27, P = 0.005) in the TLE group (Fig. 2d). In other words, decreases in outward and inward signal flow were related to lower connectome gradient values. These associations between functional gradient, and outward- (r = 0.07, P = 0.266) and inward-degree values (r = 0.20, P = 0.024) were nominally weaker in healthy controls (Fig. 2d).

3.3. Effects of Cortical Morphology and Microstructure

Consistent with previous studies (Bernhardt et al., 2010, 2008; Larivière et al., 2020a; Lin et al., 2007; McDonald et al., 2008; Whelan et al., 2018), patients with TLE exhibited cortical thinning in precentral, paracentral, superior parietal, and precuneus areas bilaterally (P_{FDR} < 0.05; Fig. 3a). However, when incorporating regional cortical atrophy profiles as a covariate in the statistical model, the effect size of functional gradient reductions in TLE remained virtually unchanged (Cohen's d = −0.47 $\pm$ 0.14; increase of Cohen's d = 2%; Fig. 3a). We also observed widespread TLE-related alterations in SWM parameters (including decreased FA and increased MD), radiating away from a temporo-limbic core to affect bilateral temporal, cingulate, lateral frontal, and posterior parietal cortices (P_{FDR} < 0.005; Fig. 3b and Figure S3). In contrast to the atrophy-corrected findings, correcting for SWM changes considerably weakened the observed functional gradient reductions in TLE (Cohen's d = −0.36 $\pm$ 0.04; reduction of Cohen's d = 21%; Fig. 3b and Figure S4). To further quantity the relationship between functional and structural alterations, we carried out a statistical mediation analysis separately using either cortical thickness or FA and MD as the mediator variable in brain regions showing significant gradient reductions (see Fig. 1d). This analysis confirmed that while TLE-related functional gradient reductions were independent of cortical atrophy (mediation effect = 0.001, P = 0.401), they were partially mediated by SWM alterations (mediation effect of FA and MD = −0.006/−0.003, P < 0.001/0.050; Fig. 3c).
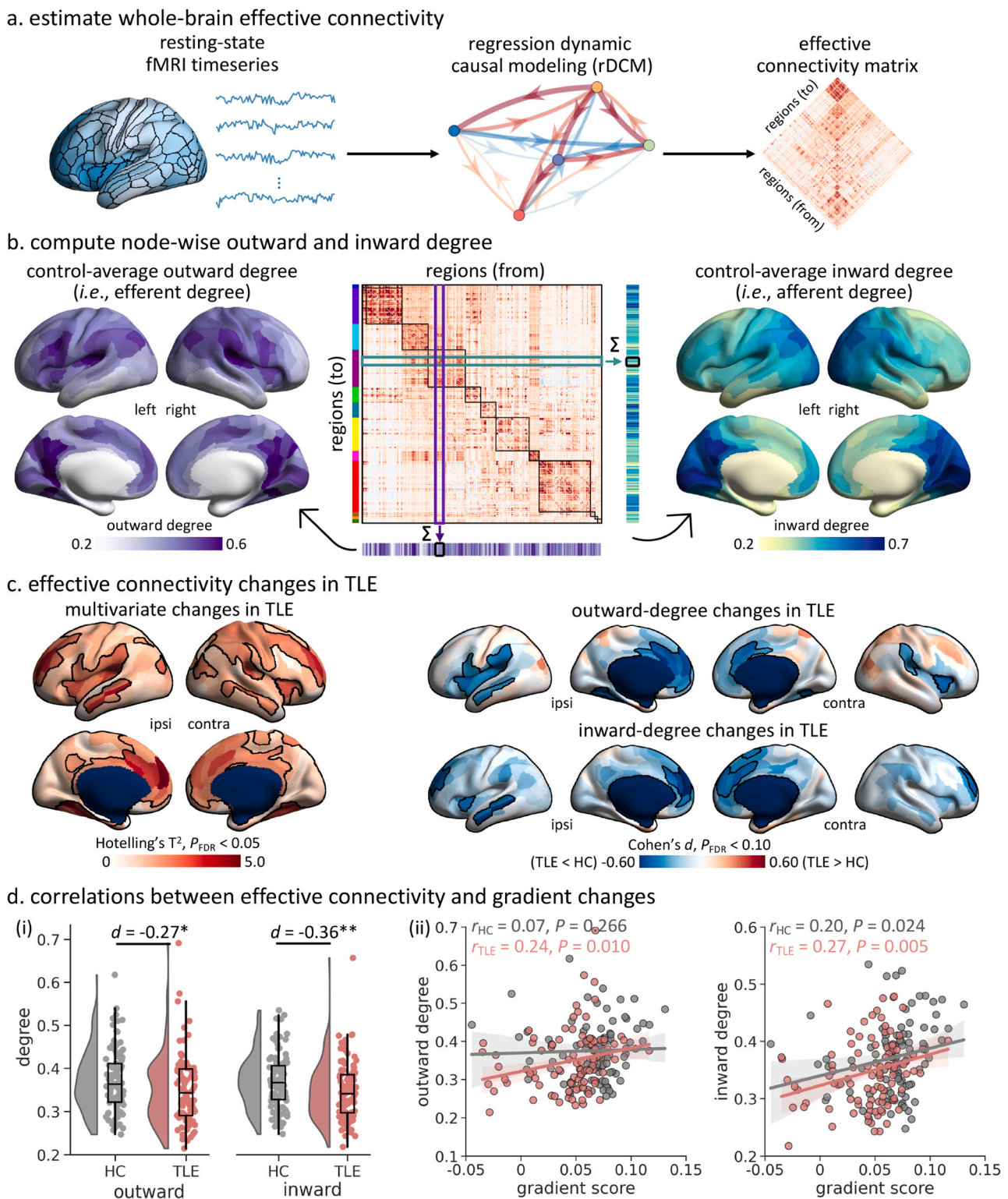
Fig. 2. Directional signal differences and correlations with gradient changes. **(a)** A schematic of estimating the effective connectivity matrix. Regression dynamic causal modelling (rDCM) was employed to estimate the whole-brain effective connectivity matrix from resting-state functional MRI data for each participant. **(b)** The node-wise outward degree (*left*) and inward degree (*right*) were determined by summarizing the unsigned EC weights (*middle*) in the columns and rows, respectively. **(c)** Univariate and multivariate analyses revealed surface-wide alterations in outward-degree and inward-degree in TLE patients compared to controls. Significant clusters, corrected for multiple comparisons using the false discovery rate procedure, are outlined in black. **(d)** Correlations between the principal gradient and directional signal flow changes. (**i**) Between-group differences in the mean outward-degree and inward-degree values. (**ii**) Across-participant correlations between the mean gradient and outward-/inward-degree values in TLE and control groups separately. Subject-specific mean gradient, outward-degree, and inward-degree values were derived from averaging regions showing significant gradient changes in Fig. 1d. * $P < 0.05$; ** $P < 0.01$. Abbreviations: *HC*, healthy controls; *TLE*, temporal lobe epilepsy; *ipsi*, ipsilateral; *contra*, contralateral.
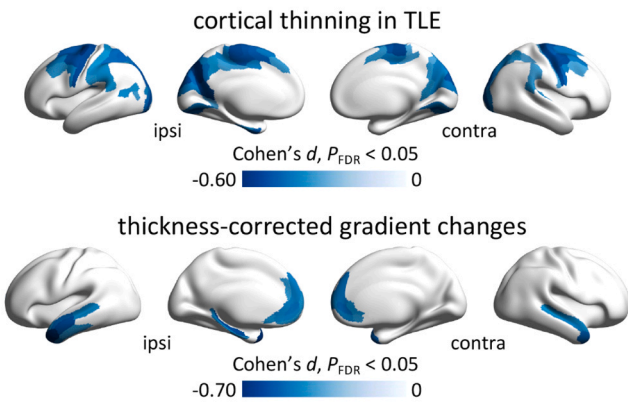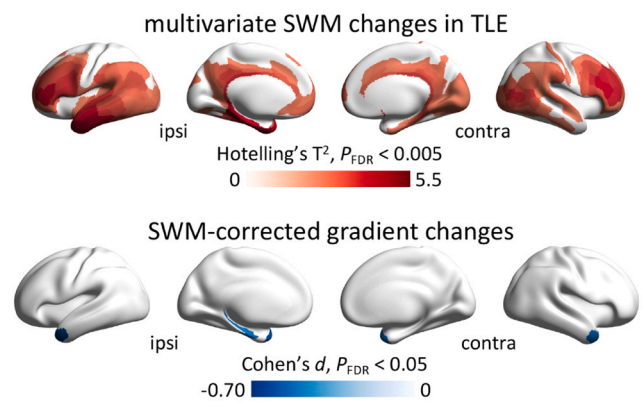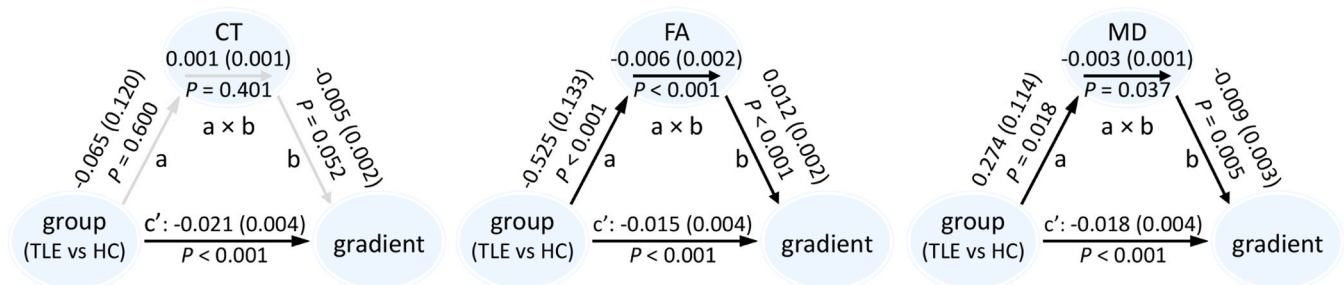
Fig. 3. Structure-function relationship. **(a)** Surface-wide between-differences in cortical thickness (CT), and the principal functional gradient (Gradient 1) after controlling for regional CT. **(b)** Surface-wide between-group differences in superficial white matter microstructural (SWM) properties (including fractional anisotropy (FA) and mean diffusivity (MD)), and the principal functional gradient after controlling for regional SWM parameters. **(c)** Mediation analyses using *group* (TLE vs. HC) as the predictive variable, *structure* (CT, FA, or MD) as the mediator variable, and *gradient* as the dependent variable. Path ***a*** indicated the effects of *group* on *structure*, path ***b*** indicated the effects of *structure* on *gradient*, and paths ***c*'** and ***a×b*** indicated the direct and the indirect/mediation effects of *group* on *gradient*, respectively. Abbreviations: *HC*, healthy controls; *TLE*, temporal lobe epilepsy; *ipsi*, ipsilateral; *contra*, contralateral.

3.4. Associations with Cognition

Our main analysis was conducted at the *MICA-MICs* site, which included three memory tests based on the episodic, semantic, and spatial memory paradigms, respectively (Sormaz et al., 2017; Tavakol et al., 2021). The results showed that TLE patients exhibited poorer memory performance compared to healthy controls, as indicated by a unified measure derived from principal component analysis (*i.e.,* PC1 score, Cohen's $d = -0.76$, $P < 0.010$). Individual memory performance positively correlated with the principal functional gradient ($r = 0.23$, $P = 0.034$), outward-degree ($r = 0.33$, $P = 0.004$), and inward-degree values ($r = 0.34$, $P = 0.004$) (Fig. 4a). That is, the greater functional topographic changes were associated with the more severe memory impairments. This relationship was further confirmed using a multi-linear regression including all three functional measures (*i.e.,* PC1 ~ gradient + outward-degree + inward-degree; $r = 0.41$, $P = 0.004$). These findings were replicated at the *EpiC* site (TLE vs. controls, Cohen's *d* for PC1 = -0.95, $P < 0.001$; principal gradient: $r = 0.21$, $P = 0.078$; outward-degree: $r = 0.22$, $P = 0.076$; inward-degree: $r = 0.20$, $P = 0.097$; multi-linear regression: $r = 0.34$, $P = 0.072$; Fig. 4b).

To support the specificity of brain-memory correlations, we also examined a complementary measure of attentional-executive ability (EpiTrack test), available at the *MICA-MICs* site (Lutz and Helmstaedter, 2005). Although TLE patients displayed lower EpiTrack scores compared to healthy controls (Cohen's $d = -0.48$, $P < 0.050$), associations between connectome alterations and EpiTrack performance were not as strong as those observed for memory (all *P*-values > 0.100; Figure S5). Additionally, *ad hoc* meta-analysis using Neurosynth confirmed that brain areas showing significant gradient reductions in

TLE were implicated in memory function (Yarkoni et al., 2011), with several higher-order cognitive and memory-related terms showing high enrichment (Figure S6).

3.5. Sensitivity, Robustness, and Replication Analyses

Several analyses supported the robustness and replicability of our main functional gradient findings.

3.5.1. Left and Right TLE
Overall findings were consistent in both left and right TLE cohorts ($rho = 0.52$, $P_{spin} < 0.001$, Figure S7). Both left (Cohen's $d = -0.58$, $P < 0.001$) and right TLE patients (Cohen's $d = -0.86$, $P < 0.001$) showed significant functional gradient reductions in bilateral temporal and medial prefrontal cortices relative to healthy controls.

3.5.2. Seizure-Free TLE
Repeating the principal functional gradient analyses in a subcohort of patients that were operated subsequently to our study, and that had histopathological validation of mesiotemporal sclerosis, and seizure-free post-surgical outcomes (*i.e.,* Engel I; $n = 32$), we found largely consistent results with our main findings ($rho = 0.88$, $P_{spin} < 0.001$), also pointing to marked gradient functional reductions in bilateral temporal and medial prefrontal cortices (Cohen's $d = -1.14$, $P < 0.001$; Figure S8).

3.5.3. Head Motion and tSNR Effects
Main gradient findings remained robust when accounting for several confounding factors. Between-group changes in the principal functional gradient were comparable when controlling for individual mean
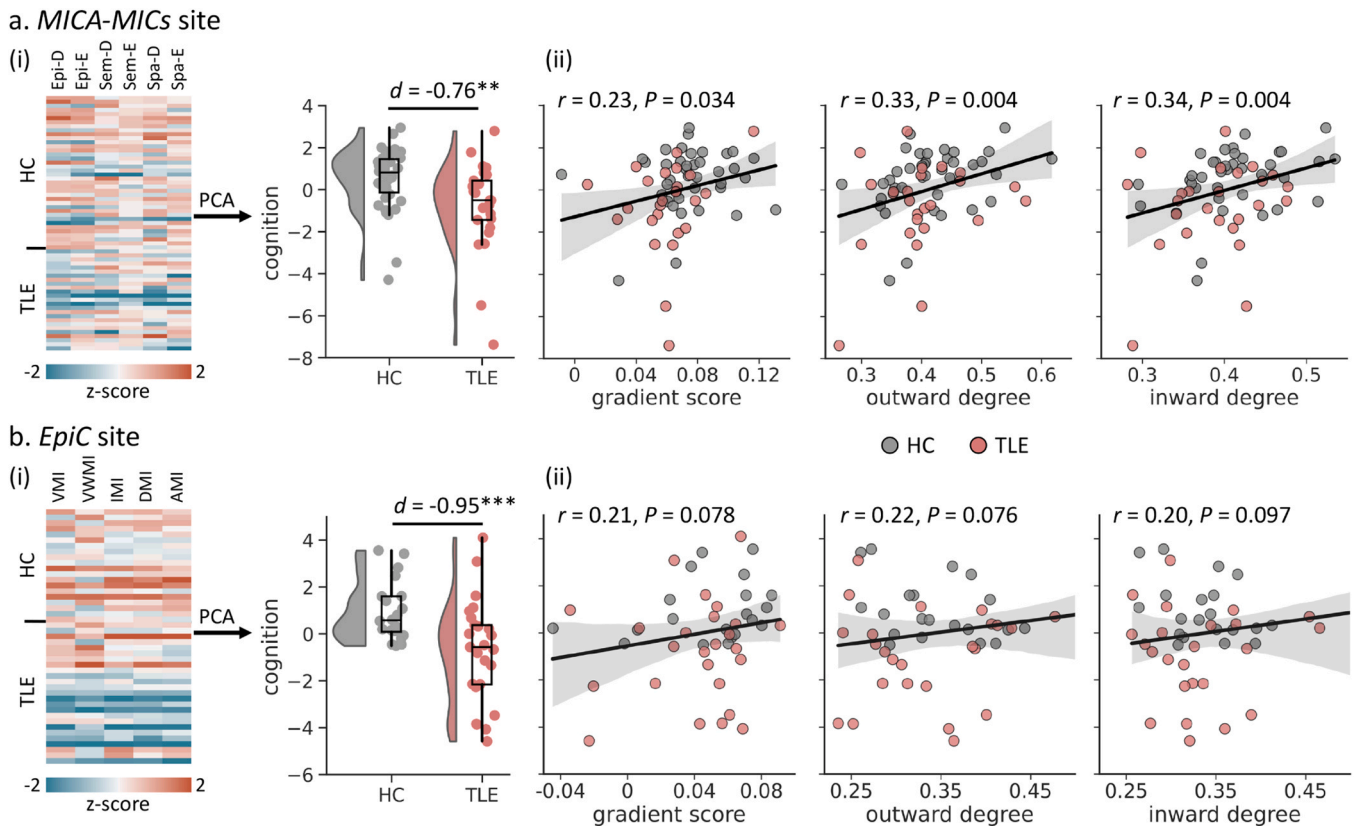
Fig. 4. Brain-memory correlations at *MICA-MICs* (a) and *EpiC* (b). **(i)** Between-group differences in the overall memory performance (*i.e.,* PC1 score) determined through principal component analyses (PCA) on various memory tests; **(ii)** Across-subject correlations between memory performance and the mean gradient, outward-degree, and inward-degree values within clusters showing significant gradient changes (Fig. 1d) after controlling for age and sex. Abbreviations: HC, healthy controls; TLE: temporal lobe epilepsy; Epi-D, episodic difficult; Epi-E, episodic easy; Sem-D, semantic difficult; Sem-E, semantic easy; Spa-D, spatial difficult; Spa-E, spatial easy; AMI, auditory memory; DMI, delayed memory; IMI, immediate memory; VMI, visual memory; VWMI, visual working memory. ** $P < 0.01$; *** $P < 0.001$.

framewise displacement (Cohen's $d = -0.41 \pm 0.05$) and regional temporal signal-to-noise ratio estimates (Cohen's $d = -0.45 \pm 0.04$; Figure S9).

3.5.4. Connectivity Matrix Thresholding

By repeatedly generating gradients based on the connectivity matrix at varying thresholds, we could replicate strong functional gradient reductions in patients with TLE in bilateral temporal and medial prefrontal cortices (Cohen's $d > -0.66$, all $P < 0.001$), and observed results which were consistent with our original findings (spatial map similarity: $rho > 0.80$, $P_{spin} < 0.001$; Figure S10).

3.5.5. Age at Seizure Onset Effects

Following the exclusion of five TLE patients with a later age at seizure onset from the *MICA-MICs* site, we observed virtually identical effect size of between-group difference in the principal functional gradient, with marked reductions in bilateral temporal and medial prefrontal cortices in patients with TLE (Cohen's $d = -0.71$, all $P < 0.001$), and the Cohen's d map exhibiting a strong correlation with that derived from the whole sample ($rho = 0.996$, $P_{spin} < 0.001$; Figure S11).

3.5.6. Interictal Epileptiform Discharges Effects

We had information on the IEDs prevalence for 33 patients at the *MICA-MICs* dataset who underwent video-EEG telemetry during their hospitalization. According to subject-specific IEDs prevalence in the temporal lobe (see Table S2), TLE patients were subdivided into three groups (11 with rare IEDs; 10 with occasional IEDs; 12 with frequent/abundant IEDs). However, no significant differences were found among

these three subgroups in the principal functional gradient ($F_{(2,30)} = 1.23$, $P = 0.306$), outward-degree ($F_{(2,30)} = 0.01$, $P = 0.998$), and inward-degree values ($F_{(2,30)} = 0.03$, $P = 0.969$) in the lateral temporal and medial prefrontal cortices (Figure S12).

3.5.7. Replication Analysis

We repeated the main analyses in an independent replication dataset (30 TLE patients and 40 healthy controls). Comparing the principal functional gradient between both cohorts, we replicated significant reductions in bilateral mesial and inferior temporal lobes as well as medial prefrontal regions in TLE patients (Cohen's $d = -0.91$, $P < 0.001$). Moreover, the spatial patterns of functional gradient changes were also significantly correlated between the discovery and replication datasets ($rho = 0.55$, $P_{spin} < 0.001$, Figure S13).

4. Discussion

This study investigated macroscale functional network organization in patients with pharmaco-resistant TLE and explored its association with cortex-wide structural compromise, as well as cognitive impairments. Using topographic gradient mapping and model-based estimation of directional signal flow patterns in a multi-site cohort of pharmaco-resistant TLE patients and controls, we discovered a significant contraction of the principal unimodal-transmodal functional gradient in the former group, particularly in bilateral temporolimbic and ventromedial prefrontal cortices. Findings were consistently observed in (i) the three study sites, (ii) patients with left or right focus, and (iii) a subcohort of patients with histologically confirmed mesiotemporal

sclerosis and post-surgical seizure freedom. Moreover, they were also replicated in an independent replication cohort of controls and TLE patients. Brain regions showing functional gradient alterations in TLE furthermore exhibited reduced signal flow to and from the rest of the brain, indicating disrupted hierarchy-dependent signaling. Additionally, by integrating multimodal MRI features in the same participants, we found that TLE-related functional reorganization was mediated by superficial white matter microstructural changes that radiated from temporolimbic regions into transmodal systems, but independent of diffuse and bilateral changes in cortical thickness. Finally, we found specific associations between functional features and individual differences in memory function, highlighting the clinical relevance of these functional changes to the commonly observed memory impairments in TLE. A series of sensitivity analyses confirmed the robustness of our findings. Taken together, our study highlights the presence of large-scale functional topographic alterations and atypical signal flow in TLE, emphasizes the mediating role of cortical microstructural changes, and suggests a relationship with the memory impairments commonly observed in the condition.

The chosen approach in the study, functional topographic gradient mapping, utilized non-linear manifold learning techniques to compress high-dimensional functional connectomes into a series of low-dimensional eigenvectors. These eigenvectors capture spatial trends in connectivity changes in a data-driven and spatially unconstrained manner. Consistent with previous studies (Margulies et al., 2016; Smallwood et al., 2021; Sydnor et al., 2021), the primary eigenvector revealed a hierarchical gradient from sensory/motor systems to transmodal association systems, representing the transition from external-oriented processing to higher-order abstract processing. Cortex-wide gradient analysis demonstrated a significant compression of the principal functional gradient in TLE patients compared to healthy controls. This indicates a reduced functional differentiation suggestive of imbalanced specialized and integrated functions in TLE (Chiang and Haneef, 2014; Lucas et al., 2023a; Park et al., 2017). Sensory-to-transmodal segregation, which supports specialized processing and integrative function, may be disrupted in TLE (Chen et al., 2017). Our findings were more prominent in lateral temporal and ventromedial prefrontal cortices, transmodal regions known to be vulnerable to TLE-related compromise (Larivière et al., 2020a, 2020b). Reductions in functional gradient values in these regions likely indicate a diminished hierarchical differentiation in connectivity profiles from other brain networks, in our case from regions at lower hierarchical levels. These findings align with previous research reporting atypical intrinsic functional signaling and altered connectivity in similar regions in TLE (Doucet et al., 2013; Fadaie et al. 2021; Girardi-Schappo et al., 2021; Liao et al., 2011; Pittau et al., 2012), and supported the notion that in TLE a lesion may affect an epileptic network rather than a circumscribed focus. Further, it may be inferred that the temporal lobe structure is a crucial part of such a network. Imbalances in short- and long-range functional connectivity in the temporo-insular cortex have been observed in earlier rs-fMRI studies, supporting that the atypical connectivity with these brain regions may result in signal flow perturbations (Larivière et al., 2020b). By showing atypical functional topography that broadly colocalizes with these cortices, our results contribute to the growing literature supporting the impact of TLE on intrinsic brain function, signaling, and macroscale functional topographic organization (Burman and Parrish, 2018; Girardi-Schappo et al., 2021; Tavakol et al., 2019).

To capture atypical signal flow in TLE, we integrated a recently developed generative model of effective connectivity, rDCM, into our analytical framework. This computationally efficient approach is well-suited for studying large networks (Frassle et al., 2021a; Frassle and Stephan, 2022). In healthy participants, we found a spatially heterogeneous distribution of regional outward and inward degree centrality. Core nodes of the default mode network, including medial parietal and lateral prefrontal regions, as well as posterior regions, exhibited higher

outward and inward degree, consistent with their role as cortical hubs (van den Heuvel and Sporns, 2013; Zuo et al., 2012). Notably, comparing inward-degree and outward-degree measures between cohorts, patients with TLE exhibited broad perturbations in signal flow across several functional systems, particularly in bilateral temporal and frontoparietal cortices. This is consistent with earlier investigations based on electroencephalography that found atypical, directed connectivity in TLE patients, affecting both specific local circuits and macroscale functional networks (Coito et al., 2016, 2019; Narasimhan et al., 2020; van Mierlo et al., 2013). Some studies based on EEG-fMRI recordings have reported that the interictal epileptiform discharges (IEDs) occurring during the resting-state may result in a relative decrease in BOLD signal in the default mode regions in TLE (Centeno and Carmichael, 2014; Laufs et al., 2007). While EEG-fMRI measures were not obtained in our cohort, we could nevertheless evaluate associations between functional measures and the IEDs prevalence estimated during video-EEG telemetry for a subset of 33 patients at the *MICA-MICs* site. Here, we observed that individual differences in functional gradient and signal flow were relatively independent of individual variations in the IEDs prevalence, suggesting that the observed alterations likely reflect a chronic functional imbalance that may not be directly linked to the frequency of transient epileptiform events (Laufs et al., 2007, 2006).

In TLE, epileptic activity may spread from the temporal lobe structures into functionally coupled brain regions, resulting in the recruitment of other neuronal assemblies (Johnson et al., 2023; Matarrese et al., 2023). The hierarchical organization of the cerebral cortex constrains the propagation of brain activity (Markov et al., 2013; Raut et al., 2021), which may explain the observed disruptions in cortical topographies, plus shifts in signal flow in TLE patients (Müller and Meisel, 2023). Indeed, associations between functional gradient and signal flow patterns were more pronounced in TLE patients than healthy individuals, indicating a pathological effect between these two complementary measures. Functional connectivity studies have identified the mesial temporal lobe (Greicius et al., 2003), and more specifically the hippocampus (Andrews-Hanna et al., 2010; Buckner and DiNicola, 2019; Genon et al., 2021; Paquola et al., 2020; Smallwood et al., 2021; Vos de Wael et al., 2018), as a key component of the human default mode network. Atypical signal flow in the default mode network in TLE could thus be the result of disturbed functional connectivity between medial temporal structures and other default mode regions. A series of rs-fMRI studies have demonstrated that functional segregation within and between the default mode network was disturbed in TLE (Caciagli et al., 2022; Larivière et al., 2020b; Li et al., 2022; Narasimhan et al., 2022; Sainburg et al., 2022; Stretton et al., 2013), suggestive of a diminished ability of surrounding brain areas to regulate activity patterns in this network. Additionally, our signal flow findings were consistent with the distributions of TLE-related decreases in cortical perfusion, controllability and network efficiency (Bernhardt et al., 2019; He et al., 2022). Intuitively, in the absence of any external input, patients with TLE required more energy costs to drive brain state transitions compared to healthy individuals. Our findings do not address the issue of causality but indicate a correlation between cortical control energy and default mode network fluctuation. A hypothetical explanation is that the energetic inefficiency in relation to TLE results in suboptimal dynamics and inadequate activation, which, in turn, eventually impair function.

Structural and diffusion-weighted MRI studies have previously reported cortical morphological changes and altered microstructure in both deep and superficial white matter in TLE patients relative to controls (Anny et al., 2019; Hatton et al., 2020; Larivière et al., 2020b; Liu et al., 2016b; Whelan et al., 2018). These alterations can disrupt the spatial arrangement of functional networks, thereby affecting hierarchical organization. In our TLE patients, the alterations in SWM microstructure followed a spatial pattern that was enriched in transmodal systems, with more pronounced effects observed in temporolimbic, prefrontal, and default mode regions compared to sensory and

unimodal cortices. Similar patterns have been reported in previous analyses of both deep and superficial white matter in TLE (Concha et al., 2012; Liu et al., 2016b), with effects often radiating away from the temporo-limbic systems, which are close to the mesiotemporal pathological core region in TLE. These findings also resemble analyses of intracortical myelin proxies, which pointed to altered microstructure and microstructural differentiation of temporo-limbic cortices (Bernhardt et al., 2018; Royer et al., 2023). Importantly, the SWM findings spatially resembled the distribution of functional gradient changes in our TLE patients, suggesting a potential mediatory role of this compartment in functional anomalies. Our *post hoc* analysis indeed confirmed that SWM changes partially mediated functional topographic findings. These findings support connectivity-based models of regional susceptibility, where regions anatomically or functionally connected to a pathological epicenter would undergo more marked alterations (Fornito et al., 2015; Larivière et al., 2020a; Shafiei et al., 2022, 2020). They also align with previous models proposing increased susceptibility of paralimbic regions to structural and functional rearrangement, possibly due to their higher potential for plasticity and connectivity reorganization (García-Cabezas et al., 2019; Park et al., 2021b). In contrast to the SWM findings, functional topographic changes were not significantly mediated by cortical thinning. This finding is consistent with earlier studies showing only a modest contribution of neocortical morphological changes to functional changes in TLE (Larivière et al., 2020b; Xie et al., 2023). The more diffused cortical gray matter changes observed beyond the mesiotemporal lobe, as revealed by between-group analyses here, may partly result from ongoing disease processes and reflect cumulative effects of seizures, anti-seizure medication, and challenges in psychosocial functioning (Caciagli et al., 2017; Coan et al., 2009; Galovic et al., 2019; Pardoe et al., 2013). These effects may be broad and less well captured by the intrinsic functional measures employed in this study, which in turn indicate a more hierarchy-specific alteration of temporal and prefrontal circuit organization.

Higher cognitive functions in humans rely on distributed network mechanisms (Bijsterbosch et al., 2020; Paquola et al., 2022; Park and Friston, 2013; Shine et al., 2019; Smallwood et al., 2021), and our study found that multiscale network-level changes in TLE were closely correlated with behavioral indices of cognitive impairment. Specifically, the more pronounced topographic gradient alterations and reduced signal flow in temporo-limbic and prefrontal cortices were associated with inter-individual differences in overall memory ability. Meta-analytical decoding further confirmed that TLE-related functional gradient alterations co-localized with regions implicated in higher, self-generated functions, including memory. Echoing their established contribution to memory in healthy individuals (Buckner and DiNicola, 2019; Buckner and Wheeler, 2001; Moscovitch et al., 2016), atypical activations of these regions in TLE patients have also been reported in prior memory task-fMRI studies (Alessio et al., 2013; Sidhu et al., 2013). Default mode regions, which are situated at maximal distances from sensory systems (Margulies et al., 2016; Oligschlager et al., 2017), provide a physical substrate for a processing route that spans from the representation of concrete stimuli to more abstract and integrative representations (Smallwood et al., 2021). This spatial arrangement also increases the divergence between large-scale systems, allowing for the formation of abstract cognition by minimizing interference from input noise (Buckner and Krienen, 2013). In our TLE patients, the reduced functional differentiation between unimodal and transmodal systems may, thus, contribute to an inefficient separation between stimulus-driven representation and internally-oriented processes, likely leading to memory dysfunction. Therefore, by situating memory functions within a topographic connectome modelling framework, our findings highlight the contributions of macroscale functional reorganization to TLE-related cognitive impairments.

Role of the Funding Source

The funders had no role in study design, data collection, analysis, interpretation, decision to publish, or manuscript preparation.

CRediT authorship contribution statement

Boris C. Bernhardt: Conceptualization, Data curation, Supervision, Writing – original draft, Writing – review & editing. **Thaera Arafat:** Data curation. **Birgit Frauscher:** Data curation, Writing – review & editing. **Lorenzo Caciagli:** Writing – review & editing. **Chifaou Abdallah:** Data curation, Writing – review & editing. **Ke Xie:** Conceptualization, Formal analysis, Investigation, Methodology, Writing – original draft, Writing – review & editing. **Linda Horwood:** Project administration. **Jessica Royer:** Data curation, Writing – review & editing. **Zhiqiang Zhang:** Data curation, Resources, Writing – review & editing. **Luis Concha:** Data curation, Resources. **Andrea Bernasconi:** Writing – review & editing. **Neda Bernasconi:** Writing – review & editing. **Donna Gift Cabalo:** Methodology, Writing – review & editing. **Alexander Ngo:** Data curation, Writing – review & editing. **Raul Rodriguez-Cruces:** Methodology, Writing – review & editing. **Stefan Frässle:** Methodology. **Shahin Tavakol:** Data curation. **Yifei Weng:** Data curation. **Jordan DeKraker:** Methodology. **Hans Auer:** Data curation. **Sara Larivière:** Methodology, Writing – review & editing.

Declaration of Generative AI and AI-Assisted Technologies in the Writing Process

The authors did not use generative AI and AI-assisted technologies in the writing process.

Declaration of Competing Interest

The authors report no competing interests.

Data Availability

The Human Connectome Project (HCP) dataset is available at https://db.humanconnectome.org/. *MICA-MICs* dataset (Royer et al., 2022b) is available at the Canadian Open Neuroscience Platform Data Portal (https://portal.conp.ca/) and the Open Science Framework (https://osf.io/j532r/). Surface-based functional connectome gradients of the study participants are available at https://osf.io/rezvy/.

Acknowledgments

Appendix A. Supporting information

Supplementary data associated with this article can be found in the online version at doi:10.1016/j.pneurobio.2024.102604.

References

Alessio, A., Pereira, F.R.S., Sercheli, M.S., Rondina, J.M., Ozelo, H.B., Bilevicius, E., et al., 2013. Brain plasticity for verbal and visual memories in patients with mesial temporal lobe epilepsy and hippocampal sclerosis: An fMRI study. Hum. Brain Mapp. 34, 186–199.

Alexander-Bloch, A.F., Shou, H., Liu, S., Satterthwaite, T.D., Glahn, D.C., Shinohara, R.T., et al., 2018. On testing for spatial correspondence between maps of human brain structure and function. NeuroImage 178, 540–551.

Anderson, K.M., Collins, M.A., Kong, R., Fang, K., Li, J., He, T., et al., 2020. Convergent molecular, cellular, and cortical neuroimaging signatures of major depressive disorder. Proc. Natl. Acad. Sci. USA 117, 25138–25149.

Andrews-Hanna, J.R., Reidler, J.S., Sepulcre, J., Poulin, R., Buckner, R.L., 2010. Functional-anatomic fractionation of the brain's default network. Neuron 65, 550–562.

Anny, R., Erik, K., Naeim, B., Akshara, B., Manu, H., Brianna, M.P., et al., 2019. Cognitive phenotypes in temporal lobe epilepsy are associated with distinct patterns of white matter network abnormalities. Neurology 92, e1957.

Avants, B.B., Tustison, N.J., Song, G., Cook, P.A., Klein, A., Gee, J.C., 2011. A reproducible evaluation of ANTs similarity metric performance in brain image registration. NeuroImage 54, 2033–2044.

Bassett, D.S., Sporns, O., 2017. Network neuroscience. Nat. Neurosci. 20, 353–364.

Bassett, D.S., Zurn, P., Gold, J.I., 2018. On the nature and use of models in network neuroscience. Nat. Rev. Neurosci. 19, 566–578.

Benjamini, Y., Hochberg, Y., 1995. Controlling the false discovery rate: a practical and powerful approach to multiple testing. J. R. Stat. Soc. 57, 289–300.

Bernasconi, N., Bernasconi, A., Caramanos, Z., Antel, S.B., Andermann, F., Arnold, D.L., 2003. Mesial temporal damage in temporal lobe epilepsy: a volumetric MRI study of the hippocampus, amygdala and parahippocampal region. Brain 126, 462–469.

Bernhardt, B.C., Bernasconi, N., Concha, L., Bernasconi, A., 2010. Cortical thickness analysis in temporal lobe epilepsy. Neurology 74, 1776.

Bernhardt, B.C., Bernasconi, A., Liu, M., Hong, S.-J., Caldairou, B., Goubran, M., et al., 2016. The spectrum of structural and functional imaging abnormalities in temporal lobe epilepsy. Ann. Neurol. 80, 142–153.

Bernhardt, B.C., Bonilha, L., Gross, D.W., 2015. Network analysis for a network disorder: The emerging role of graph theory in the study of epilepsy. Epilepsy Behav. 50, 162–170.

Bernhardt, B.C., Chen, Z., He, Y., Evans, A.C., Bernasconi, N., 2011. Graph-theoretical analysis reveals disrupted small-world organization of cortical thickness correlation networks in temporal lobe epilepsy. Cereb. Cortex 21, 2147–2157.

Bernhardt, B.C., Fadaie, F., Liu, M., Caldairou, B., Gu, S., Jefferies, E., et al., 2019. Temporal lobe epilepsy: Hippocampal pathology modulates connectome topology and controllability. Neurology 92, e2209–e2220.

Bernhardt, B.C., Fadaie, F., Vos de Wael, R., Hong, S.J., Liu, M., Guiot, M.C., et al., 2018. Preferential susceptibility of limbic cortices to microstructural damage in temporal lobe epilepsy: A quantitative T1 mapping study. NeuroImage 182, 294–303.

Bernhardt, B.C., Worsley, K.J., Besson, P., Concha, L., Lerch, J.P., Evans, A.C., et al., 2008. Mapping limbic network organization in temporal lobe epilepsy using morphometric correlations: Insights on the relation between mesiotemporal connectivity and cortical atrophy. NeuroImage 42, 515–524.

Bernhardt, B.C., Worsley, K.J., Kim, H., Evans, A.C., Bernasconi, A., Bernasconi, N., 2009. Longitudinal and cross-sectional analysis of atrophy in pharmacoresistant temporal lobe epilepsy. Neurology 72, 1747–1754.

Bijsterbosch, J., Harrison, S.J., Jbabdi, S., Woolrich, M., Beckmann, C., Smith, S., et al., 2020. Challenges and future directions for representations of functional brain organization. Nat. Neurosci. 23, 1484–1495.

Blümcke, I., Thom, M., Aronica, E., Armstrong, D.D., Bartolomei, F., Bernasconi, A., et al., 2013. International consensus classification of hippocampal sclerosis in temporal lobe epilepsy: A Task Force report from the ILAE Commission on Diagnostic Methods. Epilepsia 54, 1315–1329.

Buckner, R.L., DiNicola, L.M., 2019. The brain's default network: updated anatomy, physiology and evolving insights. Nat. Rev. Neurosci. 20, 593–608.

Buckner, R.L., Krienen, F.M., 2013. The evolution of distributed association networks in the human brain. Trends Cogn. Sci. 17, 648–665.

Buckner, R.L., Wheeler, M.E., 2001. The cognitive neuroscience og remembering. Nat. Rev. Neurosci. 2, 624–634.

Bullmore, E., Sporns, O., 2009. Complex brain networks: graph theoretical analysis of structural and functional systems. Nat. Rev. Neurosci. 10, 186–198.

Burman, R.J., Parrish, R.R., 2018. The widespread network effects of focal epilepsy. J. Neurosci. 38, 8107.

Burt, J.B., Demirtas, M., Eckner, W.J., Navejar, N.M., Ji, J.L., Martin, W.J., et al., 2018. Hierarchy of transcriptomic specialization across human cortex captured by structural neuroimaging topography. Nat. Neurosci. 21, 1251–1259.

Caciagli, L., Bernasconi, A., Wiebe, S., Koepp, M.J., Bernasconi, N., Bernhardt, B.C., 2017. A meta-analysis on progressive atrophy in intractable temporal lobe epilepsy: Time is brain? Neurology 89, 506–516.

Caciagli, L., Paquola, C., He, X., Vollmar, C., Centeno, M., Wandschneider, B., et al., 2022. Disorganization of language and working memory systems in frontal versus temporal lobe epilepsy. Brain 146, 935–953.

Centeno, M., Carmichael, D.W., 2014. Network connectivity in epilepsy: Resting state fMRI and EEG–fMRI contributions. Front Neurol. 5, 93.

Chen, Y., Wang, S., Hilgetag, C.C., Zhou, C., 2017. Features of spatial and functional segregation and integration of the primate connectome revealed by trade-off between wiring cost and efficiency. PLoS Comput. Biol. 13, e1005776.

Chiang, S., Haneef, Z., 2014. Graph theory findings in the pathophysiology of temporal lobe epilepsy. Clin. Neurophysiol. 125, 1295–1305.

Coan, A.C., Appenzeller, S., Bonilha, L., Li, L.M., Cendes, F., 2009. Seizure frequency and lateralization affect progression of atrophy in temporal lobe epilepsy. Neurology 73, 834.

Coifman, R.R., Lafon, S., Lee, A.B., Maggioni, M., Nadler, B., Warner, F., et al., 2005. Geometric diffusions as a tool for harmonic analysis and structure definition of data: Diffusion maps. Proc. Natl. Acad. Sci. USA 102, 7426–7431.

Coito, A., Genetti, M., Pittau, F., Iannotti, G.R., Thomschewski, A., Höller, Y., et al., 2016. Altered directed functional connectivity in temporal lobe epilepsy in the absence of interictal spikes: A high density EEG study. Epilepsia 57, 402–411.

Coito, A., Michel, C.M., Vulliemoz, S., Plomp, G., 2019. Directed functional connections underlying spontaneous brain activity. Hum. Brain Mapp. 40, 879–888.

Concha, L., Kim, H., Bernasconi, A., Bernhardt, B.C., Bernasconi, N., 2012. Spatial patterns of water diffusion along white matter tracts in temporal lobe epilepsy. Neurology 79, 455.

Cox, R.W., 1996. AFNI: Software for analysis and visualization of functional magnetic resonance neuroimages. Comput. Biomed. Res 29, 162–173.

Cruces, R.R., Royer, J., Herholz, P., Lariviere, S., de Wael, R.V., Paquola, C., et al., 2022. Micapipe: a pipeline for multimodal neuroimaging and connectome analysis. NeuroImage 263, 119612.

van den Heuvel, M.P., Sporns, O., 2013. Network hubs in the human brain. Trends Cogn. Sci. 17, 683–696.

Dong, H.-M., Margulies, D.S., Zuo, X.-N., Holmes, A.J., 2021. Shifting gradients of macroscale cortical organization mark the transition from childhood to adolescence. Proc. Natl. Acad. Sci. USA 118 e2024448118.

Doucet, G., Osipowicz, K., Sharan, A., Sperling, M.R., Tracy, J.I., 2013. Extratemporal functional connectivity impairments at rest are related to memory performance in mesial temporal epilepsy. Hum. Brain Mapp. 34, 2202–2216.

Fadaie, F., Lee, H.M., Caldairou, B., Gill, R.S., Sziklas, V., Crane, J., et al., 2021. Atypical functional connectome hierarchy impacts cognition in temporal lobe epilepsy. Epilepsia 62, 2589–2603.

Fischl, B., 2012. FreeSurfer. NeuroImage 62, 774–781.

Fornito, A., Zalesky, A., Breakspear, M., 2015. The connectomics of brain disorders. Nat. Rev. Neurosci. 16, 159–172.

Frassle, S., Harrison, S.J., Heinzle, J., Clementz, B.A., Tamminga, C.A., Sweeney, J.A., et al., 2021a. Regression dynamic causal modeling for resting-state fMRI. Hum. Brain Mapp. 42, 2159–2180.

Frassle, S., Manjaly, Z.M., Do, C.T., Kasper, L., Pruessmann, K.P., Stephan, K.E., 2021b. Whole-brain estimates of directed connectivity for human connectomics. NeuroImage 225, 117491.

Frassle, S., Stephan, K.E., 2022. Test-retest reliability of regression dynamic causal modeling. Netw. Neurosci. 6, 135–160.

Frässle, S., Aponte, E.A., Bollmann, S., Brodersen, K.H., Do, C.T., Harrison, O.K., et al., 2021. TAPAS: An open-source software package for translational neuromodeling and computational psychiatry. Front Psychiatry 12, 680811.

Frässle, S., Lomakina, E.I., Kasper, L., Manjaly, Z.M., Leff, A., Pruessmann, K.P., et al., 2018. A generative model of whole-brain effective connectivity. NeuroImage 179, 505–529.

Frässle, S., Lomakina, E.I., Razi, A., Friston, K.J., Buhmann, J.M., Stephan, K.E., 2017. Regression DCM for fMRI. NeuroImage 155, 406–421.

Friston, K.J., Kahan, J., Biswal, B., Razi, A., 2014. A DCM for resting state fMRI. NeuroImage 94, 396–407.

Galovic, M., van Dooren, V.Q.H., Postma, T., Vos, S.B., Caciagli, L., Borzi, G., et al., 2019. Progressive cortical thinning in patients with focal epilepsy. JAMA Neurol. 76, 1230–1239.

García-Cabezas, M.Á., Zikopoulos, B., Barbas, H., 2019. The Structural Model: a theory linking connections, plasticity, pathology, development and evolution of the cerebral cortex. Brain Struct. Funct. 224, 985–1008.

Genon, S., Bernhardt, B.C., La Joie, R., Amunts, K., Eickhoff, S.B., 2021. The many dimensions of human hippocampal organization and (dys)function. Trends Neurosci. 44, 977–989.

Girardi-Schappo, M., Fadaie, F., Lee, H.M., Caldairou, B., Sziklas, V., Crane, J., et al., 2021. Altered communication dynamics reflect cognitive deficits in temporal lobe epilepsy. Epilepsia 62, 1022–1033.

Glasser, M.F., Coalson, T.S., Robinson, E.C., Hacker, C.D., Harwell, J., Yacoub, E., et al., 2016. A multi-modal parcellation of human cerebral cortex. Nature 536, 171–178.

Glasser, M.F., Sotiropoulos, S.N., Wilson, J.A., Coalson, T.S., Fischl, B., Andersson, J.L., et al., 2013. The minimal preprocessing pipelines for the Human Connectome Project. NeuroImage 80, 105–124.

Gonzalez, H.F.J., Chakravorti, S., Goodale, S.E., Gupta, K., Claassen, D.O., Dawant, B., et al., 2019. Thalamic arousal network disturbances in temporal lobe epilepsy and improvement after surgery. J. Neurol. Neurosurg. Psychiatry 90, 1109–1116.

Goulas, A., Changeux, J.P., Wagstyl, K., Amunts, K., Palomero-Gallagher, N., Hilgetag, C. C., 2021. The natural axis of transmitter receptor distribution in the human cerebral cortex. Proc. Natl. Acad. Sci. USA 118 e2020574118.

Greicius, M.D., Krasnow, B., Reiss, A.L., Menon, V., 2003. Functional connectivity in the resting brain: A network analysis of the default mode hypothesis. Proc. Natl. Acad. Sci. USA 100, 253–258.

Greve, D.N., Fischl, B., 2009. Accurate and robust brain image alignment using boundary-based registration. NeuroImage 48, 63–72.

Gu, Y., Sainburg, L.E., Kuang, S., Han, F., Williams, J.W., Liu, Y., et al., 2021. Brain activity fluctuations propagate as waves traversing the cortical hierarchy. Cereb. Cortex 31, 3986–4005.

Han, L., Kashyap, A.L., Finin, T., Mayfield, J., Weese, J. (2013) UMBC_EBIQUITY-CORE: Semantic textual similarity systems. In: Second Joint Conference on Lexical and Computational Semantics (* SEM), Volume 1: Proceedings of the Main Conference and the Shared Task: Semantic Textual Similarity. pp. 44-52.

Hatton, S.N., Huynh, K.H., Bonilha, L., Abela, E., Alhusaini, S., Altmann, A., et al., 2020. White matter abnormalities across different epilepsy syndromes in adults: an ENIGMA-Epilepsy study. Brain 143, 2454–2473.

He, X., Caciagli, L., Parkes, L., Stiso, J., Karrer, T.M., Kim, J.Z., et al., 2022. Uncovering the biological basis of control energy: Structural and metabolic correlates of energy inefficiency in temporal lobe epilepsy. Sci. Adv. 8, eabn2293.

Hermann, B.P., Struck, A.F., Busch, R.M., Reyes, A., Kaestner, E., McDonald, C.R., 2021. Neurobehavioural comorbidities of epilepsy: towards a network-based precision taxonomy. Nat. Rev. Neurol. 17, 731–746.

Hirsch, L.J., Fong, M.W.K., Leitinger, M., LaRoche, S.M., Beniczky, S., Abend, N.S., et al., 2021. American Clinical Neurophysiology Society's Standardized Critical Care EEG Terminology: 2021 Version. J. Clin. Neurophysiol. 38.

Hong, S.J., Hyung, B., Paquola, C., Bernhardt, B.C., 2019a. The superficial white matter in autism and its role in connectivity anomalies and symptom severity. Cereb. Cortex 29, 4415–4425.

Hong, S.J., Vos de Wael, R., Bethlehem, R.A.I., Lariviere, S., Paquola, C., Valk, S.L., et al., 2019b. Atypical functional connectome hierarchy in autism. Nat. Commun. 10, 1022.

Jenkinson, M., Beckmann, C.F., Behrens, T.E.J., Woolrich, M.W., Smith, S.M., 2012. FSL. NeuroImage 62, 782–790.

Ji, G.J., Li, J., Liao, W., Wang, Y., Zhang, L., Bai, T., et al., 2022. Neuroplasticity-related genes and dopamine receptors associated with regional cortical thickness increase following electroconvulsive therapy for major depressive disorder. Mol. Neurobiol. 60, 1465–1475.

Ji, J.L., Spronk, M., Kulkarni, K., Repovš, G., Anticevic, A., Cole, M.W., 2019. Mapping the human brain's cortical-subcortical functional network organization. NeuroImage 185, 35–57.

Johnson, G.W., Doss, D.J., Morgan, V.L., Paulo, D.L., Cai, L.Y., Shless, J.S., et al., 2023. The Interictal Suppression Hypothesis in focal epilepsy: network-level supporting evidence. Brain 146, 2828–2845.

Lariviere, S., Paquola, C., Park, B.-y, Royer, J., Wang, Y., Benkarim, O., et al., 2021. The ENIGMA Toolbox: multiscale neural contextualization of multisite neuroimaging datasets. Nat. Methods 18, 698–700.

Larivière, Bayrak, S., Vos de Wael, R., Benkarim, O., Herholz, P., Rodriguez-Cruces, R., et al., 2023. BrainStat: A toolbox for brain-wide statistics and multimodal feature associations. NeuroImage 266, 119807.

Larivière, S., Rodríguez-Cruces, R., Royer, J., Caligiuri, M.E., Gambardella, A., Concha, L., et al., 2020a. Network-based atrophy modeling in the common epilepsies: A worldwide ENIGMA study. Sci. Adv. 6, eabc6457.

Larivière, S., Royer, J., Rodríguez-Cruces, R., Paquola, C., Caligiuri, M.E., Gambardella, A., et al., 2022. Structural network alterations in focal and generalized epilepsy assessed in a worldwide ENIGMA study follow axes of epilepsy risk gene expression. Nat. Commun. 13, 4320.

Larivière, S., Weng, Y., Vos de Wael, R., Royer, J., Frauscher, B., Wang, Z., et al., 2020b. Functional connectome contractions in temporal lobe epilepsy: Microstructural underpinnings and predictors of surgical outcome. Epilepsia 61, 1221–1233.

Laufs, H., Hamandi, K., Salek-Haddadi, A., Kleinschmidt, A.K., Duncan, J.S., Lemieux, L., 2007. Temporal lobe interictal epileptic discharges affect cerebral activity in "default mode" brain regions. Hum. Brain Mapp. 28, 1023–1032.

Laufs, H., Lengler, U., Hamandi, K., Kleinschmidt, A., Krakow, K., 2006. Linking generalized spike-and-wave discharges and resting state brain activity by using EEG/fMRI in a patient with absence seizures. Epilepsia 47, 444–448.

Li, R., Deng, C., Wang, X., Zou, T., Biswal, B., Guo, D., et al., 2022. Interictal dynamic network transitions in mesial temporal lobe epilepsy. Epilepsia 63, 2242–2255.

Li, Q., Tavakol, S., Royer, J., Lariviere, S., Vos De Wael, R., Park, B.Y., et al., 2021. Atypical neural topographies underpin dysfunctional pattern separation in temporal lobe epilepsy. Brain 144, 2486–2498.

Liao, W., Zhang, Z., Pan, Z., Mantini, D., Ding, J., Duan, X., et al., 2011. Default mode network abnormalities in mesial temporal lobe epilepsy: A study combining fMRI and DTI. Hum. Brain Mapp. 32, 883–895.

Lin, J.J., Mula, M., Hermann, B.P., 2012. Uncovering the neurobehavioural comorbidities of epilepsy over the lifespan. Lancet 380, 1180–1192.

Lin, J.J., Salamon, N., Lee, A.D., Dutton, R.A., Geaga, J.A., Hayashi, K.M., et al., 2007. Reduced neocortical thickness and complexity mapped in mesial temporal lobe epilepsy with hippocampal sclerosis. Cereb. Cortex 17, 2007–2018.

Liu, M., Bernhardt, B.C., Bernasconi, A., Bernasconi, N., 2016a. Gray matter structural compromise is equally distributed in left and right temporal lobe epilepsy. Hum. Brain Mapp. 37, 515–524.

Liu, M., Bernhardt, B.C., Hong, S.J., Caldairou, B., Bernasconi, A., Bernasconi, N., 2016b. The superficial white matter in temporal lobe epilepsy: a key link between structural and functional network disruptions. Brain 139, 2431–2440.

Lucas, A., Cornblath, E.J., Sinha, N., Hadar, P., Caciagli, L., Keller, S.S., et al., 2023a. Resting state functional connectivity demonstrates increased segregation in bilateral temporal lobe epilepsy. Epilepsia 64, 1305–1317.

Lucas, A., Mouchtaris, S., Cornblath, E.J., Sinha, N., Caciagli, L., Hadar, P., et al., 2023b. Subcortical functional connectivity gradients in temporal lobe epilepsy. Neuroimage Clin. 38, 103418.

Lutz, M.T., Helmstaedter, C., 2005. EpiTrack: Tracking cognitive side effects of medication on attention and executive functions in patients with epilepsy. Epilepsy Behav. 7, 708–714.

Maccotta, L., He, B.J., Snyder, A.Z., Eisenman, L.N., Benzinger, T.L., Ances, B.M., et al., 2013. Impaired and facilitated functional networks in temporal lobe epilepsy. Neuroimage Clin. 2, 862–872.

Margulies, D.S., Ghosh, S.S., Goulas, A., Falkiewicz, M., Huntenburg, J.M., Langs, G., et al., 2016. Situating the default-mode network along a principal gradient of macroscale cortical organization. Proc. Natl. Acad. Sci. USA 113, 12574–12579.

Markov, N.T., Ercsey-Ravasz, M., Van Essen, D.C., Knoblauch, K., Toroczkai, Z., Kennedy, H., 2013. Cortical high-density counterstream architectures. Science 342, 1238406.

Markov, N.T., Kennedy, H., 2013. The importance of being hierarchical. Curr. Opin. Neurobiol. 23, 187–194.

Markov, N.T., Vezoli, J., Chameau, P., Falchier, A., Quilodran, R., Huissoud, C., et al., 2014. Anatomy of hierarchy: Feedforward and feedback pathways in macaque visual cortex. J. Comp. Neurol. 522, 225–259.

Matarrese, M.A.G., Loppini, A., Fabbri, L., Tamilia, E., Perry, M.S., Madsen, J.R., et al., 2023. Spike propagation mapping reveals effective connectivity and predicts surgical outcome in epilepsy. Brain 146, 3898–3912.

McDonald, C.R., Hagler Jr, D.J., Ahmadi, M.E., Tecoma, E., Iragui, V., Gharapetian, L., et al., 2008. Regional neocortical thinning in mesial temporal lobe epilepsy. Epilepsia 49, 794–803.

Meng, Y., Yang, S., Chen, H., Li, J., Xu, Q., Zhang, Q., et al., 2021. Systematically disrupted functional gradient of the cortical connectome in generalized epilepsy: Initial discovery and independent sample replication. NeuroImage 230, 117831.

van Mierlo, P., Carrette, E., Hallez, H., Raedt, R., Meurs, A., Vandenberghe, S., et al., 2013. Ictal-onset localization through connectivity analysis of intracranial EEG signals in patients with refractory epilepsy. Epilepsia 54, 1409–1418.

Moscovitch, M., Cabeza, R., Winocur, G., Nadel, L., 2016. Episodic memory and beyond: the hippocampus and neocortex in transformation. Annu Rev. Psychol. 67, 105.

Müller, P.M., Meisel, C., 2023. Spatial and temporal correlations in human cortex are inherently linked and predicted by functional hierarchy, vigilance state as well as antiepileptic drug load. PLoS Comput. Biol. 19 e1010919.

Murphy, K., Birn, R.M., Bandettini, P.A., 2013. Resting-state fMRI confounds and cleanup. NeuroImage 80, 349–359.

Narasimhan, S., Gonzalez, H.F.J., Johnson, G.W., Wills, K.E., Paulo, D.L., Morgan, V.L., et al., 2022. Functional connectivity between mesial temporal and default mode structures may help lateralize surgical temporal lobe epilepsy. J. Neurosurg. 137, 1571–1581.

Narasimhan, S., Kundassery, K.B., Gupta, K., Johnson, G.W., Wills, K.E., Goodale, S.E., et al., 2020. Seizure-onset regions demonstrate high inward directed connectivity during resting-state: An SEEG study in focal epilepsy. Epilepsia 61, 2534–2544.

Oligschlager, S., Huntenburg, J.M., Golchert, J., Lauckner, M.E., Bonnen, T., Margulies, D.S., 2017. Gradients of connectivity distance are anchored in primary cortex. Brain Struct. Funct. 222, 2173–2182.

Paquola, C., Amunts, K., Evans, A., Smallwood, J., Bernhardt, B., 2022. Closing the mechanistic gap: the value of microarchitecture in understanding cognitive networks. Trends Cogn. Sci. 26, 873–886.

Paquola, C., Benkarim, O., DeKraker, J., Lariviere, S., Frassle, S., Royer, J., et al., 2020. Convergence of cortical types and functional motifs in the human mesiotemporal lobe. eLife 9 e60673.

Paquola, C., Hong, S.-J., 2022. The potential of myelin-sensitive imaging: Redefining spatiotemporal patterns of myeloarchitecture. Biol. Psychiatry 93, 442–454.

Paquola, C., Vos De Wael, R., Wagstyl, K., Bethlehem, R.A.I., Hong, S.J., Seidlitz, J., et al., 2019. Microstructural and functional gradients are increasingly dissociated in transmodal cortices. PLoS Biol. 17 e3000284.

Pardoe, H.R., Berg, A.T., Jackson, G.D., 2013. Sodium valproate use is associated with reduced parietal lobe thickness and brain volume. Neurology 80, 1895.

Park, C.-h, Choi, Y.S., Jung, A.R., Chung, H.-K., Kim, H.J., Yoo, J.H., et al., 2017. Seizure control and memory impairment are related to disrupted brain functional integration in temporal lobe epilepsy. J. Neuropsychiatry Clin. Neurosci. 29, 343–350.

Park, H.J., Friston, K., 2013. Structural and functional brain networks: from connections to cognition. Science 342, 1238411.

Park, B.-y, Hong, S.-J., Valk, S.L., Paquola, C., Benkarim, O., Bethlehem, R.A.I., et al., 2021a. Differences in subcortico-cortical interactions identified from connectome and microcircuit models in autism. Nat. Commun. 12, 2225.

Park, Larivière, B.-y, Rodríguez-Cruces, S., Royer, R., Tavakol, J., Wang, S., Y, et al., 2021b. Topographic divergence of atypical cortical asymmetry and atrophy patterns in temporal lobe epilepsy. Brain 145, 1285–1298.

Park, B.-y, Paquola, C., Bethlehem, R.A.I., Benkarim, O., Mišić, B., Smallwood, J., et al., 2022. Adolescent development of multiscale structural wiring and functional interactions in the human connectome. Proc. Natl. Acad. Sci. USA 119.

Park, B.-y, Park, H., Morys, F., Kim, M., Byeon, K., Lee, H., et al., 2021c. Inter-individual body mass variations relate to fractionated functional brain hierarchies. Commun. Biol. 4, 735.

Pittau, F., Grova, C., Moeller, F., Dubeau, F., Gotman, J., 2012. Patterns of altered functional connectivity in mesial temporal lobe epilepsy. Epilepsia 53, 1013–1023.

Power, J.D., Mitra, A., Laumann, T.O., Snyder, A.Z., Schlaggar, B.L., Petersen, S.E., 2014. Methods to detect, characterize, and remove motion artifact in resting state fMRI. NeuroImage 84, 320–341.

Raut, R.V., Snyder, A.Z., Mitra, A., Yellin, D., Fujii, N., Malach, R., et al., 2021. Global waves synchronize the brain's functional systems with fluctuating arousal. Sci. Adv. 7 eabf2709.

Rodriguez-Cruces, R., Bernhardt, B.C., Concha, L., 2020. Multidimensional associations between cognition and connectome organization in temporal lobe epilepsy. NeuroImage 213, 116706.

Rodriguez-Cruces, R., Royer, J., Larivière, S., Bassett, D.S., Caciagli, L., Bernhardt, B.C., 2022. Multimodal connectome biomarkers of cognitive and affective dysfunction in the common epilepsies. Netw. Neurosci. 6, 320–338.

Rodriguez-Cruces, R., Velázquez-Pérez, L., Rodríguez-Leyva, I., Velasco, A.L., Trejo-Martínez, D., Barragán-Campos, H.M., et al., 2018. Association of white matter diffusion characteristics and cognitive deficits in temporal lobe epilepsy. Epilepsy Behav. 79, 138–145.

Royer, J., Bernhardt, B.C., Larivière, S., Gleichgerrcht, E., Vorderwülbecke, B.J., Vulliémoz, S., et al., 2022a. Epilepsy and brain network hubs. Epilepsia 63, 537–550.

Royer, J., Larivière, S., Rodriguez-Cruces, R., Cabalo, D.G., Tavakol, S., Auer, H., et al., 2023. Cortical microstructural gradients capture memory network reorganization in temporal lobe epilepsy. Brain 146, 3923–3937.

Royer, J., Rodríguez-Cruces, R., Tavakol, S., Lariviere, S., Herholz, P., Li, Q., et al., 2022b. An open MRI dataset for multiscale neuroscience. Sci. Data 9, 569.

Sainburg, L.E., Little, A.A., Johnson, G.W., Janson, A.P., Levine, K.K., González, H.F.J., et al., 2022. Characterization of resting functional MRI activity alterations across epileptic foci and networks. Cereb. Cortex.

Salimi-Khorshidi, G., Douaud, G., Beckmann, C.F., Glasser, M.F., Griffanti, L., Smith, S.M., 2014. Automatic denoising of functional MRI data: Combining independent component analysis and hierarchical fusion of classifiers. NeuroImage 90, 449–468.

Shafiei, G., Bazinet, V., Dadar, M., Manera, A.L., Collins, D.L., Dagher, A., et al., 2022. Network structure and transcriptomic vulnerability shape atrophy in frontotemporal dementia. Brain 146, 321–336.

Shafiei, G., Markello, R.D., Makowski, C., Talpalaru, A., Kirschner, M., Devenyi, G.A., et al., 2020. Spatial patterning of tissue volume loss in schizophrenia reflects brain network architecture. Biol. Psychiatry 87, 727–735.

Shahin, T., Valeria, K., Jessica, R., Qiongling, L., Hans, A., Jordan, D., et al., 2022. Differential Memory Impairment Across Relational Domains in Temporal Lobe Epilepsy. bioRxiv, 2022.2011.2001.514752.

Shine, J.M., Breakspear, M., Bell, P.T., Ehgoetz Martens, K.A., Shine, R., Koyejo, O., et al., 2019. Human cognition involves the dynamic integration of neural activity and neuromodulatory systems. Nat. Neurosci. 22, 289–296.

Sidhu, M.K., Stretton, J., Winston, G.P., Bonelli, S., Centeno, M., Vollmar, C., et al., 2013. A functional magnetic resonance imaging study mapping the episodic memory encoding network in temporal lobe epilepsy. Brain 136, 1868–1888.

Smallwood, J., Bernhardt, B.C., Leech, R., Bzdok, D., Jefferies, E., Margulies, D.S., 2021. The default mode network in cognition: a topographical perspective. Nat. Rev. Neurosci. 22, 503–513.

Sormaz, M., Jefferies, E., Bernhardt, B.C., Karapanagiotidis, T., Mollo, G., Bernasconi, N., et al., 2017. Knowing what from where: Hippocampal connectivity with temporoparietal cortex at rest is linked to individual differences in semantic and topographic memory. NeuroImage 152, 400–410.

Stasenko, A., Lin, C., Bonilha, L., Bernhardt, B.C., McDonald, C.R., 2022. Neurobehavioral and clinical comorbidities in epilepsy: The role of white matter network disruption. Neuroscientist, 10738584221076133.

Stretton, J., Winston, G.P., Sidhu, M., Bonelli, S., Centeno, M., Vollmar, C., et al., 2013. Disrupted segregation of working memory networks in temporal lobe epilepsy. Neuroimage Clin. 2, 273–281.

Sydnor, V.J., Larsen, B., Bassett, D.S., Alexander-Bloch, A., Fair, D.A., Liston, C., et al., 2021. Neurodevelopment of the association cortices: Patterns, mechanisms, and implications for psychopathology. Neuron 109, 2820–2846.

Sydnor, V.J., Larsen, B., Seidlitz, J., Adebimpe, A., Alexander-Bloch, A.F., Bassett, D.S., et al., 2023. Intrinsic activity development unfolds along a sensorimotor–association cortical axis in youth. Nat. Neurosci. 26, 638–649.

Tavakol, S., Li, Q., Royer, J., Vos de Wael, R., Larivière, S., Lowe, A., et al., 2021. A structure–function substrate of memory for spatial configurations in medial and lateral temporal cortices. Cereb. Cortex 31, 3213–3225.

Tavakol, S., Royer, J., Lowe, A.J., Bonilha, L., Tracy, J.I., Jackson, G.D., et al., 2019. Neuroimaging and connectomics of drug-resistant epilepsy at multiple scales: From focal lesions to macroscale networks. Epilepsia 60, 593–604.

Téllez-Zenteno, J.F., Hernández-Ronquillo, L., 2012. A review of the epidemiology of temporal lobe epilepsy. Epilepsy Res Treat. 2012, 630853.

Valk, S.L., Di Martino, A., Milham, M.P., Bernhardt, B.C., 2015. Multicenter mapping of structural network alterations in autism. Hum. Brain Mapp. 36, 2364–2373.

Valk, S.L., Xu, T., Paquola, C., Park, B.-y, Bethlehem, R.A.I., Vos de Wael, R., et al., 2022. Genetic and phylogenetic uncoupling of structure and function in human transmodal cortex. Nat. Commun. 13, 2341.

Van Essen, D.C., Glasser, M.F., Dierker, D.L., Harwell, J., Coalson, T., 2012. Parcellations and hemispheric asymmetries of human cerebral cortex analyzed on surface-based atlases. Cereb. Cortex 22, 2241–2262.

Van Essen, D.C., Smith, S.M., Barch, D.M., Behrens, T.E.J., Yacoub, E., Ugurbil, K., 2013. The WU-Minn Human Connectome Project: An overview. NeuroImage 80, 62–79.

Váša, F., Mišić, B., 2022. Null models in network neuroscience. Nat. Rev. Neurosci. 23, 493–504.

Vezoli, J., Magrou, L., Goebel, R., Wang, X.-J., Knoblauch, K., Vinck, M., et al., 2021. Cortical hierarchy, dual counterstream architecture and the importance of top-down generative networks. NeuroImage 225, 117479.

Vos de Wael, R., Benkarim, O., Paquola, C., Lariviere, S., Royer, J., Tavakol, S., et al., 2020. BrainSpace: a toolbox for the analysis of macroscale gradients in neuroimaging and connectomics datasets. Commun. Biol. 3, 103.

Vos de Wael, R., Larivière, S., Caldairou, B., Hong, S.J., Margulies, D.S., Jefferies, E., et al., 2018. Anatomical and microstructural determinants of hippocampal subfield functional connectome embedding. Proc. Natl. Acad. Sci. USA 115, 10154–10159.

Wang, Y., Royer, J., Park, B.Y., Vos de Wael, R., Larivière, S., Tavakol, S., et al., 2022. Long-range functional connections mirror and link microarchitectural and cognitive hierarchies in the human brain. Cereb. Cortex 33, 1782–1798.

Weng, Y., Lariviere, S., Caciagli, L., Vos de Wael, R., Rodriguez-Cruces, R., Royer, J., et al., 2020. Macroscale and microcircuit dissociation of focal and generalized human epilepsies. Commun. Biol. 3, 244.

Whelan, C.D., Altmann, A., Botia, J.A., Jahanshad, N., Hibar, D.P., Absil, J., et al., 2018. Structural brain abnormalities in the common epilepsies assessed in a worldwide ENIGMA study. Brain 141, 391–408.

Xia, M., Liu, J., Mechelli, A., Sun, X., Ma, Q., Wang, X., et al., 2022. Connectome gradient dysfunction in major depression and its association with gene expression profiles and treatment outcomes. Mol. Psychiatry 27, 1384–1393.

Xie, K., Royer, J., Lariviere, S., Rodriguez-Cruces, R., de Wael, R.V., Park, B.-y, et al., 2023. Atypical intrinsic neural timescales in temporal lobe epilepsy. Epilepsia 64, 998–1011.

Yarkoni, T., Poldrack, R.A., Nichols, T.E., Van Essen, D.C., Wager, T.D., 2011. Large-scale automated synthesis of human functional neuroimaging data. Nat. Methods 8, 665–670.

Yasuda, C.L., Chen, Z., Beltramini, G.C., Coan, A.C., Morita, M.E., Kubota, B., et al., 2015. Aberrant topological patterns of brain structural network in temporal lobe epilepsy. Epilepsia 56, 1992–2002.

Yeo, B.T., Krienen, F.M., Sepulcre, J., Sabuncu, M.R., Lashkari, D., Hollinshead, M., et al., 2011. The organization of the human cerebral cortex estimated by intrinsic functional connectivity. J. Neurophysiol. 106, 1125–1165.

Yousefi, B., Keilholz, S., 2021. Propagating patterns of intrinsic activity along macroscale gradients coordinate functional connections across the whole brain. NeuroImage 231, 117827.

Zuo, X.N., Ehmke, R., Mennes, M., Imperati, D., Castellanos, F.X., Sporns, O., et al., 2012. Network centrality in the human functional connectome. Cereb. Cortex 22, 1862–1875.